Quantitative Susceptibility Mapping at 3 T and 1.5 T: Evaluation of Consistency and Reproducibility.

AUTHOR(S):

Hinoda, Takuya; Fushimi, Yasutaka; Okada, Tomohisa; Fujimoto, Koji; Liu, Chunlei; Yamamoto, Akira; Okada, Tsutomu; Kido, Aki; Togashi, Kaori

CITATION:

Hinoda, Takuya ...[et al]. Quantitative Susceptibility Mapping at 3 T and 1.5 T: Evaluation of Consistency and Reproducibility.. Investigative radiology 2015, 50(8): 522-530

ISSUE DATE:

2015-04-18

URL:

http://hdl.handle.net/2433/197533

Title Page

Manuscript Title

Quantitative Susceptibility Mapping at 3T and 1.5T: Evaluation of Consistency and Reproducibility

Takuya Hinoda, MD [1)], Yasutaka Fushimi, MD, PhD [1)], Tomohisa Okada, MD, PhD [1)], Koji Fujimoto, MD, PhD [1)], Chunlei Liu, PhD [2)], Akira Yamamoto, MD, PhD [1)], Tsutomu Okada, MD, PhD [1)], Aki Kido, MD, PhD [1)], Kaori Togashi, MD, PhD [1)]

1) Department of Diagnostic Imaging and Nuclear Medicine, Kyoto University Graduate School of Medicine.

54 Shogoin Kawaharacho, Sakyoku, Kyoto, JAPAN 6068507

2) Brain Imaging and Analysis Center and Department of Radiology, Duke University Medical Center.

2424 Erwin Road, Suite 501, Durham, NC 27705

Corresponding author

Yasutaka Fushimi, MD, PhD

Department of Diagnostic Imaging and Nuclear Medicine

Graduate School of Medicine, Kyoto University

54 Shogoinkawaharacho, Sakyo, Kyoto, 606-8507, Japan

Office phone: +81-75-751-3760

Office FAX: +81-75-771-9709

e-mail:yfushimi@kuhp.kyoto-u.ac.jp

Acknowledgement

This work was supported by JSPS KAKENHI Grant Number 25461815 and a sponsored research program, “Researches for improvement of MR visualization (No. 150100700014)” provided to one of the authors, Professor Kaori Togashi, by Toshiba Medical Systems Corporation, Japan. The authors are grateful to Kyoko Takakura, RT for her support.

Short title

QSM at 3T and 1.5T

Acknowledgement

This work was supported by JSPS KAKENHI Grant Number 25461815 and a sponsored research program, “Researches for improvement of MR visualization (No. 150100700014)” provided to one of the authors, Professor Kaori Togashi, by Toshiba Medical Systems Corporation, Japan. The authors are grateful to Kyoko Takakura, RT for her support.

Abstracts

Objectives: To assess the consistency and reproducibility of quantitative susceptibility mapping (QSM) at 3T and 1.5T MR scanners.

Materials and Methods: This study was approved by institutional ethics committee and written informed consent was obtained. Twenty-two healthy volunteers underwent two examinations on different days. Each examination consisted of MR imaging at both 3T and 1.5T MR scanners. The data from both scanners and examination days were obtained, and QSM was calculated with STI Suite using two different algorithms: HARmonic PhasE RemovaL using

LAplacian operator (HARPERELLA) and a SHARP method with a variable radius of the spherical kernel at the brain boundary (V-SHARP). We evaluated consistency of QSM between 3T and 1.5T, and the reproducibility between the 1st and 2nd examinations using two phase processing methods (HARPERELLA and V-SHARP).

Results: Susceptibility values of regions of interests at 3T were highly correlated with those at 1.5T with good agreement (HARPERELLA: R^2=0.838, V-SHARP: R^2=0.898) (average difference ±1.96 standard deviation; HARPERELLA: -0.012±0.046, V-SHARP: -0.002±0.034). Reproducibility analysis demonstrated excellent correlation between the 1st and 2nd examination at both 3T and 1.5T for both algorithms (HARPERELLA at 3T: R^2=0.921, 1.5T: R^2=0.891; V-SHARP at 3T: R^2=0.937, 1.5T: R^2=0.926). Bland-Altman analysis showed excellent reproducibility for HARPERELLA (at 3T: -0.003±0.032, 1.5T: -0.003±0.038) and V-SHARP (at 3T: -0.003±0.027, 1.5T: -0.003±0.029). Susceptibility values of these two algorithms were highly correlated with good agreement (3T: R^2=0.961, 1.5T: R^2=0.931) (3T: 0.009±0.023, 1.5T: -0.003±0.049).

Conclusion: QSM with HARPERELLA and V-SHARP demonstrated good reproducibility at 3T and 1.5T, and QSM with V-SHARP demonstrated good consistency at 3T and 1.5T.

Key words

Magnetic Resonance Imaging;

Quantitative Susceptibility Mapping;

HARmonic PhasE RemovaL using LAplacian operator;

variable radius of the spherical kernel at the brain boundary;

Text

Introduction

Quantitative Susceptibility Mapping (QSM) is a novel post-processing technique that uses gradient echo phase images to directly measure tissue magnetic susceptibility caused by various sources such as iron, myelin and physiological calcification [1-4]. Phase images have provided good tissue contrast and allowed the detection of intrinsic iron content changes [5, 6], however, phase images are influenced by background phase originating objects outside of a region of interest as well as phase wrapping [7, 8]. In comparison, QSM provides a more intrinsic measure of tissue magnetic susceptibility and has become a promising tool [4, 9-15].

Susceptibility values calculated from QSM have been reported to have a strong correlation with iron concentration in human brain especially in deep gray matter structures [14, 16-18]. Abnormal concentration of iron stores in human brain was demonstrated in various neurological diseases, for example in the basal ganglia and active demyelinating lesion for multiple sclerosis [19], in hippocampus and cerebral cortex for Alzheimer's disease [20, 21], and in substantia nigra for Parkinson's disease [22]. It has been shown that QSM provides excellent depiction of brain lesions in a number of neurologic diseases and disorders, including microbleeds [23], multiple sclerosis [24, 25], brain tumors [26], intracranial calcifications and hemorrhages [27], and neurodegenerative diseases [28-30].

QSM of human brain has already been applied to research and clinical applications at various field strength including 7T, 3T and 1.5T. Currently, near all clinical MR scans are performed at 3T and 1.5T. However, to our knowledge, no reports have focused on the comparison of susceptibility values at 3T and 1.5T, nor the reproducibility on each static magnetic field. Because QSM is a quantitative measurement, we

hypothesized that QSM values measured at 3T and 1.5T should be equivalent in the same subjects. Therefore, the purpose of this study was to assess the consistency of magnetic susceptibility of human brains between 3T and 1.5T MR scanners, using STI Suite provided by Duke University which has been considerably applied to research and clinical imaging [8]. We also investigated the reproducibility of susceptibility values at each MR scanner and the association between two different algorithms for background phase removal in calculating QSM. We acknowledge that there are a growing number of QSM algorithms available and it is not realistic to evaluate all existing methods in a single study. However, as different algorithms improve, their results are expected to converge thus the main findings of this study will hold as the algorithms become more mature. Accordingly, the purpose of this study was to assess the consistency and reproducibility of QSM at 3T and 1.5T MR scanners.

Materials and Methods

Phantom preparation

A gadolinium (Gd) phantom was constructed for in-vitro validation study to measure susceptibility values in comparison with theoretical values. 2% agarose gels in spherical form (diameter 2.5cm) with various concentration of gadoterate meglumine (Gd-DOTA) (Dotarem, Guerbet, Villepinte, France) were fixed in a cubic container filled with water. Gd agarose gels contained Gd concentration of 0.25%, 0.5%, 0.75%, 1.0%, 1.25%, and 1.5%, corresponding to theoretical susceptibility values of 0.41 ppm, 0.81 ppm, 1.22 ppm, 1.63 ppm, 2.04 ppm, and 2.45 ppm[31]. MR imaging was conducted at both 3T and 1.5T MR scanner.

Human subjects

This prospective study was approved by the institutional ethics committee and a written informed consent was obtained for each participant, and 22 healthy volunteers were enrolled (17 men, 5 women; age range, 23–41 years; mean age, 30.2 years ± 5.2 [standard deviation]). All subjects underwent 2 examinations on different days. Each examination consists of MR imaging at both 3T and 1.5T MR scanners on a single day without delays: Specifically, MR imaging was conducted at 3T first, then, subsequently at 1.5T immediately after the 3T scan on the 1st examination day. On the 2nd examination day, MR imaging was conducted at 1.5T first, then at 3T. The interval between the 1st and 2nd examination was maintained at around 20 days. None of the volunteers had a history of neurologic, psychiatric, ophthalmologic or cardiovascular diseases.

MR imaging

MR imaging was performed on a 3T scanner (Vantage, Toshiba Medical Systems, Otawara, Japan) using a 32-channel head coil and on a 1.5T scanner (Excelart Vantage Powered by Atlas, Toshiba Medical Systems, Otawara, Japan) using a 12-channel head coil.

Three-dimensional (3D) gradient-echo images for QSM calculation were acquired for the Gd phantom and human subjects at both 3T and 1.5T using a 3D single-echo T2*-weighted field echo sequence with the following parameters: repetition time (TR), 60 msec; echo time (TE), 40 msec; flip angle, 20°; resolution, 1 × 1 × 1 mm; a parallel imaging factor of 3 in phase-encoding direction. The acquisition time was 14 minutes and 26 seconds. For anatomical reference of human subjects, 3D T1-weighted IR prepared fast field echo images (TR, 5.9 msec; TE, 2.7 msec; inversion time, 900 msec; flip angle, 9°; resolution, 1.2 × 1 × 1.2 mm; parallel imaging factor of 2 in phase-encoding direction and 1.5 in slice direction; acquisition time,

5 minutes 47 seconds) were also acquired at 3T. These T1-weighted images were used for brain segmentation and Diffeomorphic Anatomical Registration using Exponentiated Lie Algebra (DARTEL) template [32].

Image processing for Gd phantom

QSM calculation was conducted from the phase of 3D gradient echo images in STI Suite version 2.10 (http://people.duke.edu/~cl160/). Mask images were generated from magnitude images by threshold for background phase removal. For phase unwrapping and back ground phase removal, we conducted two different algorithms: (i) integrated phase unwrapping and background phase removal by HARmonic PhasE RemovaL using LAplacian operator (HARPERELLA) method, and (ii) a SHARP method with a variable radius of the spherical kernel at the brain boundary (V-SHARP) [8, 14]. QSM with HARPERELLA and QSM with V-SHARP were then calculated from each local tissue phase by solving an inverse problem using the iLSQR method (an algorithm for sparse linear equations and sparse least squares) [8, 33]. The strength of the static magnetic field was calculated from the central frequency and gyromagnetic ratio of water of each MR scan.

QSM with HARPERELLA and QSM with V-SHARP at the 3T and 1.5T were compared with the theoretical susceptibility values respectively. QSM values were compared between 3T and 1.5T to evaluate consistency of susceptibility values.

Image Processing for human subjects

The process of calculating and creating QSM images in Montreal Neurological Institute (MNI) space (http://www.mni.mcgill.ca/) for human subjects is outlined in Fig. 1. QSM calculation was conducted from the phase of 3D gradient echo images in STI Suite version 2.10. Skull stripped brain masks were generated

from magnitude images with Brain Extraction tool (BET), FSL (http://www.fmrib.ox.ac.uk/fsl/) for background phase removal [34]. We conducted the HARPERELLA method and the V-SHARP method [8, 14]. QSM with HARPERELLA and QSM with V-SHARP were then calculated from each local tissue phase by the iLSQR method[8]. The strength of the static magnetic field was calculated from the central frequency and gyromagnetic ratio of water of each MR scan.

3D T1-weighted images were co-registered to the corresponding magnitude images by using SPM8 software (Wellcome Department of Imaging Neuroscience, University College London, UK) implemented in MATLAB 2013b (Mathworks, Natick, Massachusetts, US). A DARTEL template was generated from the entire image dataset using DARTEL import files. In the next step, all co-registered 3D T1-weighted images were mapped to the MNI space using nonlinear warping [32]. QSM images were transformed into MNI space with a Gaussian filter (full width at half maximum [1, 1, 1 mm]) by using DARTEL imported files and normalized QSM images with 1-mm isotropic voxel were created (Fig. 2).

Regions of interest for human subjects

A single set of regions of interest (ROIs) was manually created by a neuroradiologist (6 years of experience [rater A]) in consultation with another neuroradiologist (17 years of experience [rater B]) on the averaged normalized QSM images of all the subjects: caudate head, putamen, globus pallidus, internal capsule, red nucleus, substantia nigra, and dentate nucleus, using the ImageJ software (National Institutes of Health, Bethesda, MD, USA) (Fig. 3). This set of ROIs was applied to the individual QSM maps derived from HARPERELLA and V-SHARP method for the 1st and 2nd examinations at 3T and 1.5T. Susceptibility values were calculated as the magnetic susceptibility in parts per million (ppm) for all voxels identified in each ROI

projected onto each individual QSM maps. In addition to the single set of ROIs on normalized QSM images, ROIs on individual original QSM images were created to check the validity of the susceptibility values between original QSM images and normalized QSM images. In particular, to assess the intra- and interobserver variability, rater A and rater B respectively created ROIs on individual original QSM images, and rater A created the other ROIs in two-week interval.

Consistency analysis of QSM between 3T and 1.5T

The total 44 QSM maps derived with HARPERELLA from both the 1st and 2nd examinations at 3T were compared with those at 1.5T by using the single set of ROIs on normalized QSM images defined above. QSM maps derived with V-SHARP were compared between 3T and 1.5T in the same way.

Reproducibility analysis of QSM between 1st and 2nd examinations

In this analysis, the total 22 QSM maps at 3T of the 1st examinations and those of the 2nd examinations were compared with respect to each QSM phase processing methods (HARPERELLA and V-SHARP) by using ROIs described above. In the same way, QSM maps at 1.5T were also compared.

Comparison analysis of QSM between HARPERELLA and V-SHARP methods

The total 44 QSM maps derived with HARPERELLA from both the 1st and 2nd examinations at 3T were compared with the corresponding QSM maps derived with V-SHARP at 3T. The same ROIs described above were used. Similarly at 1.5T, QSM maps derived with HARPERELLA were compared with the corresponding QSM maps derived with V-SHARP.

Statistical analysis

All statistical analyses were conducted by using MedCalc version 13.3 (MedCalc Software bvba,

Ostend, Belgium). Susceptibility values of phantom experiments were assessed using regression analysis (slope, R^2). Susceptibility values of the single set of ROIs were assessed using regression analysis (slope, R^2) and Bland-Altman analysis of 95% limits of agreement (average difference ± 1.96 standard deviation of the difference). Intra- and interobserver variability using interclass correlation coefficients (ICC) was evaluated by the single set of ROIs on normalized QSM and the manual ROIs on the individual original QSM of rater A (first time [#1]), (second time [#2]) and rater B, and Bland-Altman plots of 95% limits of agreement (average difference ± 1.96 standard deviation of the difference) were conducted between the single set of ROIs and the manual ROIs which were mean of the rater A and rater B.

Results

Phantom experiments

QSM images of the Gd phantom at each MR scanner were shown in Fig. 4. Susceptibility values of each spherical Gd agarose gel were correlated with the theoretical susceptibility values derived from Gd concentration (see Figure, Supplemental Digital Content 1): HARPERELLA at 3T: slope = 0.990, R^2 = 0.977; 3T, V-SHARP at 3T: slope = 0.960, R^2 = 0.995; HARPERELLA at 1.5T: slope =1.059, R^2 = 0.981; V-SHARP at 1.5T: slope = 1.006, R^2 = 0.991. In addition, excellent consistency was demonstrated between 3T and 1.5T: HARPERELLA: slope = 0.934, R^2 = 0.995; V-SHARP: slope = 1.048, R^2 = 0.997.

Region of interest for human subjects

Susceptibility values of the single set of ROIs derived from HARPERELLA and V-SHARP of the 22 subjects averaged at 2 time points are shown in Table 1 for both 3T and 1.5T. Data are presented as mean ±

standard deviation.

Mean susceptibility values by the single set of ROIs and each rater were shown in Figure, Supplemental Digital Content 2. Intraobserver agreement rates were as follows: HARPERELLA at 3T: 0.961 (95% confidence interval [CI]: 0.954, 0.966), V-SHARP at 3T: 0.966 (95% CI: 0.961, 0.971), HARPERELLA at 1.5T: 0.974 (95% CI: 0.970, 0.978), V-SHARP at 1.5T: 0.970 (95% CI: 0.965, 0.974). Interobserver agreement rates were as follows: HARPERELLA at 3T: 0.948 (95% CI: 0.941, 0.954), V-SHARP at 3T: 0.950 (95% CI: 0.944, 0.956), HARPERELLA at 1.5T: 0.944 (95% CI: 0.937, 0.951), V-SHARP at 1.5T: 0.949 (95% CI: 0.942, 0.955). Bland-Altman analysis also showed excellent agreement between the raters on original QSM and the single set of ROIs on normalized QSM: HARPERELLA at 3T: -0.003 ppm ± 0.037, V-SHARP at 3T: -0.001 ppm ± 0.036, HARPERELLA at 1.5T: 0.003 ppm ± 0.041, V-SHARP at 1.5T: 0.004 ppm ± 0.032.

Consistency analysis of QSM between 3T and 1.5T

Susceptibility values with HARPERELLA at 3T were highly correlated with those at 1.5T (slope = 0.899, R^2 = 0.838) (Fig. 5a). Susceptibility values with V-SHARP at 3T were also highly correlated with those at 1.5T (slope = 0.964, R^2 = 0.898) (Fig. 5b). QSM with V-SHARP was better correlated between the two field strengths than was QSM with HARPERELLA. Bland-Altman analysis showed good agreement in QSM with HARPERELLA (-0.012 ppm ± 0.046) (Fig. 5c) and better agreement with V-SHARP (-0.002 ppm ± 0.034) (Fig. 5d).

Reproducibility analysis of QSM between 1st and 2nd examinations

Susceptibility values of the 1st study and the 2nd study were also highly correlated at both magnets (QSM with HARPERELLA at 3T: slope = 0.950, R^2 =0.921 (Fig. 6a); at 1.5T: slope = 0.965, R^2 = 0.891 (Fig.

6b)) (QSM with V-SHARP at 3T: slope = 0.971, R^2 = 0.937 (Fig. 6c); at 1.5T: slope = 0.969, R^2 = 0.926 (Fig. 6d)). Bland-Altman analysis showed excellent agreement for both methods at both fields: HARPERELLA at 3T (-0.003 ppm ± 0.032) (Fig. 6e) and 1.5T (-0.003 ppm ± 0.038) (Fig. 6f); V-SHARP at 3T (-0.003 ppm ± 0.027) (Fig. 6g) and 1.5T (-0.003 ppm ± 0.029) (Fig. 6h).

Comparison analysis of QSM between HARPERELLA and V-SHARP methods

Susceptibility values derived from these two different background phase removal algorithms were compared with each other. QSM with HARPERELLA were also highly correlated with QSM with V-SHARP (3T: slope = 0.924, R^2 = 0.961 (Fig. 7a); 1.5T: slope = 0.878, R^2 = 0. 931 (Fig. 7b)). Bland-Altman analysis also showed good agreement between the two algorithms at 3T (0.009 ppm ± 0.023) (Fig. 7c) and 1.5T (-0.003 ppm ± 0.049) (Fig. 7d).

Discussion

The result of Gd phantom experiments and consistency analysis of QSM between 3T and 1.5T in human subjects showed good correlation with little variance of susceptibility values for both HARPERELLA and V-SHARP methods. Magnetic susceptibility of a given object is theoretically an invariable value independent of static magnetic fields, therefore susceptibility values at 3T and 1.5T should be theoretically identical. This study has confirmed our initial hypothesis that susceptibility values measured at 3T and 1.5T should be equivalent in the same subject to be true. Phase unwrapping was well conducted and consistent QSM results were achieved with the single-echo sequence which might cause phase unwrapping error and phase variation due to the B1 variation. Background fields resulting from paranasal sinus and mastoid air cells

are much severer at 3T than 1.5T, however, our results demonstrated that susceptibility values derived with HARPERELLA and V-SHARP at both magnets were in good agreement in spite of unfavorable circumstances of background field at 3T. Our results support that QSM is a reliable quantification method to measure magnetic susceptibility longitudinally at different magnets, and probably more consistently with the V-SHARP method compared to HARPERELLA.

Reproducibility of susceptibility values in human subjects over two time points was excellent both at 3T and at 1.5T and for both the HARPERELLA and the V-SHARP method. This excellent reproducibility indicates that both algorithms are reliable for serial evaluation of susceptibility values with limited variance. High reproducibility of susceptibility values is important for longitudinal tissue evaluation and for comparison study between normal controls and patients. Although reproducibility of QSM at 3T scanners was assessed [36], there have been no prior reports demonstrating the consistency and reproducibility of QSM at different static magnetic fields, therefore, our data provide the critical evidences suggesting good reproducibility of QSM for clinical usage.

Comparison analysis of QSM between HARPERELLA and V-SHARP methods revealed good correlation between the two different algorithms. Since reproducible results were demonstrated in both algorithms throughout this study, both algorithms were consistent with each other with high reproducibility. Previous report demonstrated that HARPERELLA is a robust technique for phase unwrapping and back ground phase removal and preserves the low spatial frequency components of the brain tissue which is important for QSM [8]. HARPERELLA preserves the Laplacian of the phase image outside the brain by using L2 norm minimization, on the contrary, V-SHARP method was conducted after the Laplacian-based phase

unwrapping where the phase Laplacian outside the brain was assumed to be zero [8]. In addition, V-SHARP method was conducted with smaller radius of the spherical kernel at the brain boundary compared with those in the center of the brain [14]. Some phase differences around the brain structure and blood vessels located on the surface were observed due to the differences of the two algorithms, which may be the reason of the slightly decreased correlation between HARPERELLA and V-SHARP.

QSM has been developed as a valuable tool for imaging and quantifying tissue magnetic properties. Although previous Gd phantom experiments were mainly performed using multi-echo sequences, our Gd phantom experiments using the single-echo sequence shows excellent correlation with the theoretical susceptibility values. Previous Cadaver studies have demonstrated a strong correlation between QSM and iron concentration of deep gray matter calculated from age [16, 18]. In this study, although the estimated iron content in deep gray matters were in good correspondence to QSM values of each ROIs in the deep gray matter (data not shown), the relationship between QSM and iron derived from cadavers might be different from that in living human being. The reproducibility of QSM in live subjects cannot be evaluated with phantoms or cadavers because magnetic susceptibility varies with physical conditions [37].

Susceptibility reference is an unresolved issue for QSM. In some studies, cerebrospinal fluid (CSF) was used as the reference [12, 17], however, susceptibility values of CSF are heterogeneous [18]. The ventricles are not homogenous structures with blood vessels, choroid plexus, small size and complicated shapes susceptible to partial volume effects; in addition, CSF flow and its composition of lipids and proteins can affect its magnetic susceptibility values. Other studies set the susceptibility in white matter to 0 ppm or -0.03 ppm as reference [13, 18]. Susceptibility values of white matter, however, is also non-uniform and easily vary, because of

myelination and anisotropy of white matter affects QSM values. In this study, we did not calibrate susceptibility values with CSF space or white matter, but our study demonstrates good consistency. Further studies are needed to optimize the calibration methods of QSM.

There are some limitations in this study. First, all ROIs were manually created on averaged QSM maps of all the subjects. Theoretically, the single set of ROIs works for all the subjects because all the QSM maps were normalized in MNI space, and susceptibility values of manual ROIs on individual QSM showed excellent correspondence to the single set of ROIs regardless of MNI transformation. Second, we evaluated only the posterior limb of internal capsule and no other white matter structures were evaluated. It is well known that fiber orientation heavily affect magnetic susceptibility of white matter [9]. Because of this anisotropy, white matter in general is not appropriate for ROI based analysis. The posterior limb of internal capsule is a suitable ROI due to its relatively consistent orientation with respect to the magnetic field. Third, subjects of this study are relatively young and the number of subjects is relatively small. Further studies of various age group and larger number of subjects are required. Fourth, Signal to noise ratio (SNR) at 3T is better than that at 1.5T, which has not been taken into consideration in this study, however, susceptibility values at 1.5T were almost equal to those at 3T in spite of lower SNR at 1.5T. Fifth, some orientation differences among subjects and examinations may exist, which might have affected the results of QSM [12]. Reproducible head positioning may lead to better consistency and reproducibility of QSM. Finally, we compared only two phase processing methods and only with STI Suite. However, it is reasonable to project that, as the algorithms improve, other state-of-the-art QSM techniques should provide similarly consistent and reproducible results. The goal of our study was not meant to provide an exhaustive comparisons of the ever growing number of QSM algorithms.

Rather, it serves to illustrate that the principles behind QSM are able to produce consistency and reproducibility values between different time points and between different magnets.

In conclusion, QSM with HARPERELLA and V-SHARP demonstrated good reproducibility at 3T and 1.5T, and QSM with V-SHARP demonstrated good consistency at 3T and 1.5T.

References

1. Reichenbach JR. The future of susceptibility contrast for assessment of anatomy and function. *Neuroimage*. 2012;62:1311-1315.
2. Haacke EM, Cheng NY, House MJ, et al. Imaging iron stores in the brain using magnetic resonance imaging. *Magn Reson Imaging*. 2005;23:1-25.
3. Liu C, Li W, Johnson GA, et al. High-field (9.4 T) MRI of brain dysmyelination by quantitative mapping of magnetic susceptibility. *Neuroimage*. 2011;56:930-938.
4. Shmueli K, de Zwart JA, van Gelderen P, et al. Magnetic susceptibility mapping of brain tissue in vivo using MRI phase data. *Magn Reson Med*. 2009;62:1510-1522.
5. Hammond KE, Lupo JM, Xu D, et al. Development of a robust method for generating 7.0 T multichannel phase images of the brain with application to normal volunteers and patients with neurological diseases. *Neuroimage*. 2008;39:1682-1692.
6. Lee J, Hirano Y, Fukunaga M, et al. On the contribution of deoxy-hemoglobin to MRI gray-white matter phase contrast at high field. *Neuroimage*. 2010;49:193-198.
7. Duyn JH, van Gelderen P, Li TQ, et al. High-field MRI of brain cortical substructure based on signal phase. *Proc Natl Acad Sci U S A*. 2007;104:11796-11801.
8. Li W, Avram AV, Wu B, et al. Integrated Laplacian-based phase unwrapping and background phase removal for quantitative susceptibility mapping. *NMR Biomed*. 2014;27:219-227.
9. Li W, Wu B, Avram AV, et al. Magnetic susceptibility anisotropy of human brain in vivo and its molecular underpinnings. *Neuroimage*. 2012;59:2088-2097.
10. Liu T, Spincemaille P, de Rochefort L, et al. Calculation of susceptibility through multiple orientation sampling (COSMOS): a method for conditioning the inverse problem from measured magnetic field map to susceptibility source image in MRI. *Magn Reson Med*. 2009;61:196-204.
11. de Rochefort L, Liu T, Kressler B, et al. Quantitative susceptibility map reconstruction from MR phase data using bayesian regularization: validation and application to brain imaging. *Magn Reson Med*. 2010;63:194-206.
12. Schweser F, Deistung A, Lehr BW, et al. Quantitative imaging of intrinsic magnetic tissue properties using MRI signal phase: an approach to in vivo brain iron metabolism? *Neuroimage*. 2011;54:2789-2807.
13. Wharton S, Schafer A, Bowtell R. Susceptibility mapping in the human brain using threshold-based k-space division. *Magn Reson Med*. 2010;63:1292-1304.
14. Wu B, Li W, Guidon A, et al. Whole brain susceptibility mapping using compressed sensing. *Magn Reson Med*. 2012;67:137-147.
15. Liu T, Liu J, de Rochefort L, et al. Morphology enabled dipole inversion (MEDI) from a single-angle acquisition: comparison with COSMOS in human brain imaging. *Magn Reson Med*. 2011;66:777-783.
16. Langkammer C, Schweser F, Krebs N, et al. Quantitative susceptibility mapping (QSM) as a means to measure brain iron? A post mortem validation study. *Neuroimage*. 2012;62:1593-1599.
17. Bilgic B, Pfefferbaum A, Rohlfing T, et al. MRI estimates of brain iron concentration in normal aging using quantitative susceptibility mapping. *Neuroimage*. 2012;59:2625-2635.
18. Lim IA, Faria AV, Li X, et al. Human brain atlas for automated region of interest selection in quantitative

susceptibility mapping: application to determine iron content in deep gray matter structures. *Neuroimage*. 2013;82:449-469.

19. Khalil M, Teunissen C, Langkammer C. Iron and neurodegeneration in multiple sclerosis. *Mult Scler Int*. 2011;2011:606807.
20. Raven EP, Lu PH, Tishler TA, et al. Increased iron levels and decreased tissue integrity in hippocampus of Alzheimer's disease detected in vivo with magnetic resonance imaging. *J Alzheimers Dis*. 2013;37:127-136.
21. Dedman DJ, Treffry A, Candy JM, et al. Iron and aluminium in relation to brain ferritin in normal individuals and Alzheimer's-disease and chronic renal-dialysis patients. *Biochem J*. 1992;287 (Pt 2):509-514.
22. Gorell JM, Ordidge RJ, Brown GG, et al. Increased iron-related MRI contrast in the substantia nigra in Parkinson's disease. *Neurology*. 1995;45:1138-1143.
23. Liu T, Surapaneni K, Lou M, et al. Cerebral microbleeds: burden assessment by using quantitative susceptibility mapping. *Radiology*. 2012;262:269-278.
24. Langkammer C, Liu T, Khalil M, et al. Quantitative susceptibility mapping in multiple sclerosis. *Radiology*. 2013;267:551-559.
25. Chen W, Gauthier SA, Gupta A, et al. Quantitative susceptibility mapping of multiple sclerosis lesions at various ages. *Radiology*. 2014;271:183-192.
26. Deistung A, Schweser F, Wiestler B, et al. Quantitative susceptibility mapping differentiates between blood depositions and calcifications in patients with glioblastoma. *PLoS One*. 2013;8:e57924.
27. Chen W, Zhu W, Kovanlikaya I, et al. Intracranial calcifications and hemorrhages: characterization with quantitative susceptibility mapping. *Radiology*. 2014;270:496-505.
28. Lotfipour AK, Wharton S, Schwarz ST, et al. High resolution magnetic susceptibility mapping of the substantia nigra in Parkinson's disease. *J Magn Reson Imaging*. 2012;35:48-55.
29. Fritzsch D, Reiss-Zimmermann M, Trampel R, et al. Seven-tesla magnetic resonance imaging in Wilson disease using quantitative susceptibility mapping for measurement of copper accumulation. *Invest Radiol*. 2014;49:299-306.
30. Tan H, Liu T, Wu Y, et al. Evaluation of iron content in human cerebral cavernous malformation using quantitative susceptibility mapping. *Invest Radiol*. 2014;49:498-504.
31. de Rochefort L, Brown R, Prince MR, et al. Quantitative MR susceptibility mapping using piece-wise constant regularized inversion of the magnetic field. *Magn Reson Med*. 2008;60:1003-1009.
32. Ashburner J. A fast diffeomorphic image registration algorithm. *Neuroimage*. 2007;38:95-113.
33. Li W, Wang N, Yu F, et al. A method for estimating and removing streaking artifacts in quantitative susceptibility mapping. *Neuroimage*. 2015;108:111-122.
34. Smith SM. Fast robust automated brain extraction. *Hum Brain Mapp*. 2002;17:143-155.
35. Liu C, Li W, Tong KA, et al. Susceptibility-weighted imaging and quantitative susceptibility mapping in the brain. *J Magn Reson Imaging*. 2014.
36. Lin PY, Chao TC, Wu ML. Quantitative Susceptibility Mapping of Human Brain at 3T: A Multisite Reproducibility Study. *AJNR Am J Neuroradiol*. 2014.
37. Schenck JF. The role of magnetic susceptibility in magnetic resonance imaging: MRI magnetic

compatibility of the first and second kinds. *Med Phys*. 1996;23:815-850.

Figure Legends

Figure 1

Flowchart for calculating and normalizing QSM with HARPERELLA and V-SHARP. (1) Phase unwrapping and back ground phase removal was conducted for the phase images of 3D gradient echo images with HARPRELLA or V-SHARP method. (2) Skull stripped magnitude images of 3D gradient echo images by using BET tool were applied to the process of (1) as brain masks. (3) QSM was calculated from tissue phase images by using iLSQR to solve ill posed inverse problem. (4) DARTEL template was calculated by 3D T1-weighted images. (5) QSM was transformed into MNI space using the DARTEL template.

Figure 2

Average and normalized QSM images of all subjects at the level of the cerebellum, brain stem, and basal ganglia: (a) QSM at 3T with HARPERELLA and (b) with V-SHARP, and (c) QSM at 1.5T with HARPERELLA and (d) with V-SHARP.

Figure 3

A common set of regions of interests was created on the averaged and normalized QSM images: caudate nucleus, putamen, globus pallidus, and posterior limb of internal capsule at the level of the basal ganglia, substantia nigra and red nucleus in the brain stem, and dentate nucleus in the cerebellum.

Figure 4

QSM images of Gd Phantom (agarose gels contained Gd concentration of 0.25%, 0.5%, 0.75%, 1.0%, 1.25%, and 1.5%, corresponding to susceptibility values of 0.41 ppm, 0.81 ppm, 1.22 ppm, 1.63 ppm, 2.04 ppm, and 2.45 ppm). (a) QSM at 3T with HARPERELLA, (b) with V-SHARP, (c) QSM at 1.5T with HARPERELLA, (d) with V-SHARP and (e) T2-weighted image.

Figure 5

Scattered plots and Bland-Altman plots of the consistency analysis of susceptibility values between 3T and 1.5T. Scattered plots show linear regression analysis of (a) susceptibility values with HARPERELLA between 3T and 1.5T and (b) susceptibility values with V-SHARP. Solid lines in the top panel indicate linear regression lines (slope). Bland-Altman plots show mean susceptibility difference between 3T and 1.5T and limits of agreement (± 1.96 standard deviation, dash lines) for the assessment of (c) susceptibility values with HARPERELLA between 3T and 1.5T, and (d) with V-SHARP between 3T and 1.5T.

Figure 6

Scattered plots and Bland-Altman plots of reproducibility analysis of susceptibility values between 1st and 2nd examinations. Scattered plots show linear regression analysis of (a) susceptibility values with HARPERELLA between the 1st and 2nd examination at 3T, (b) with HARPERELLA at 1.5T, (c) with V-SAHRP at 3T, and, (d) with V-SHARP at 1.5T. Solid lines indicate linear regression (slope). Bland-Altman plots show mean susceptibility difference between the 1st and 2nd examination and limits of agreement (±

1.96 standard deviation, dash lines) for the assessment of (e) susceptibility values with HARPERELLA at 3T, (f) with HARPERELLA at 1.5T, (g) with V-SHARP at 3T, and, (h) with V-SHARP at 1.5T.

Figure 7

Scattered plots and Bland-Altman plots of comparison analysis of susceptibility values between HARPERELLA and V-SHARP. Scattered plots show linear regression analysis of (a) susceptibility values between HARPERELLA and V-SHARP methods at 3T and (b) at 1.5T. Solid lines indicate linear regression (slope). Bland-Altman plots show mean susceptibility difference between HARPERELLA and V-SHARP and limits of agreement (± 1.96 standard deviation, dash lines) for the assessment of (c) susceptibility values between HARPERELLA and V-SHARP method at 3T and (d) at 1.5T.

Table 1

Susceptibility values and standard deviation per region of interest. Mean ± SD. [ppm]

	HARPERELLA (3T)	V-SHARP (3T)	HARPERELLA (1.5T)	V-SHARP (1.5T)
Caudate Nucleus	0.042 ± 0.017	0.038 ± 0.011	0.037 ± 0.019	0.038 ± 0.012
Dentate Nucleus	0.084 ± 0.025	0.071 ± 0.022	0.094 ± 0.024	0.070 ± 0.020
Globus Pallidus	0.141 ± 0.024	0.123 ± 0.020	0.129 ± 0.024	0.130 ± 0.021
Putamen	0.063 ± 0.015	0.052 ± 0.011	0.050 ± 0.017	0.053 ± 0.012
Red Nucleus	0.071 ± 0.029	0.068 ± 0.026	0.048 ± 0.025	0.056 ± 0.022
Substantia nigra	0.100 ± 0.024	0.093 ± 0.018	0.073 ± 0.028	0.083 ± 0.021
Internal Capsule	-0.042 ± 0.012	-0.051 ± 0.010	-0.056 ± 0.016	-0.047 ± 0.012

Supplemental Digital Content 1

Scattered plots of the region of interest analysis. Scattered plots show linear regression analysis with theoretical susceptibility values of (a) measured susceptibility values at 3T with HARPERELLA, (b) with V-SHARP, (c) at 1.5T with HARPERELLA, and (d) with V-SHARP. Linear regression analysis between 3T and 1.5T (e) with HARPERELLA and (f) V-SHARP.

Supplemental Digital Content 2

Mean susceptibility values by the single set of ROIs and each rater on (a) QSM with HARPERELLA at 3T, (b) with V-SHARP at 3T, (c) with HARPERELLA at 1.5T and (d) with V-SHARP at 1.5T.

Fig.1
Click here to download high resolution image

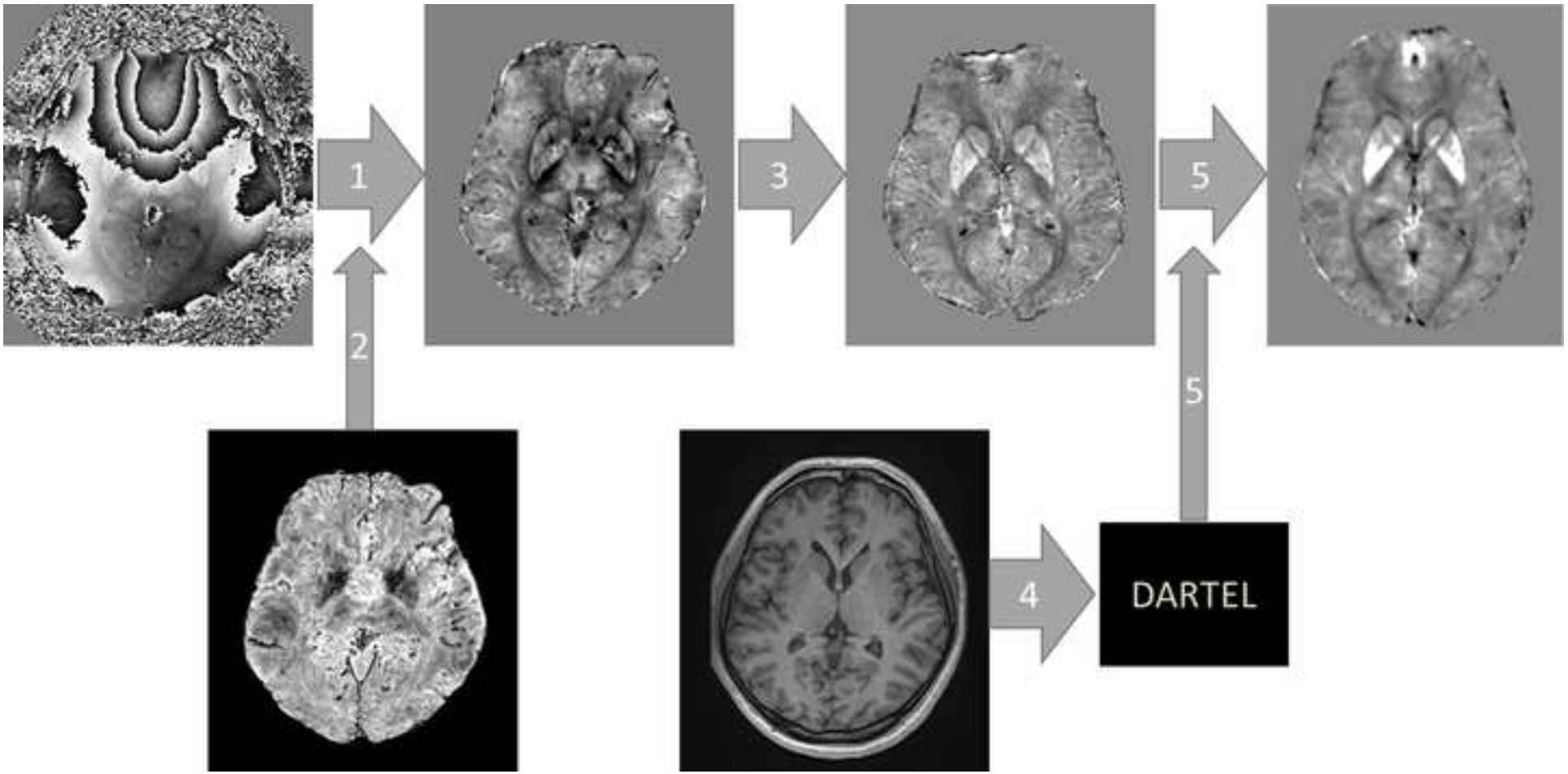

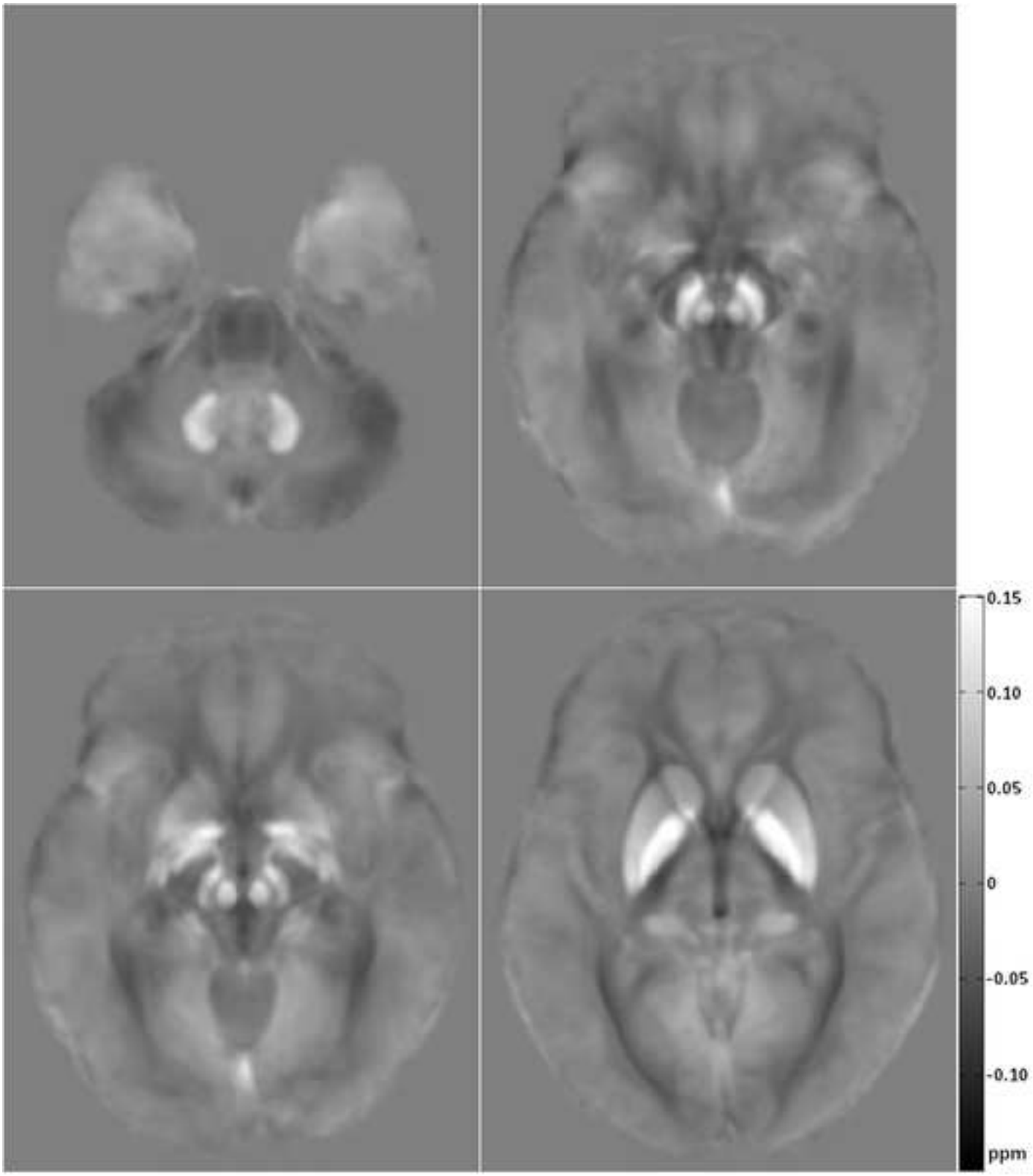

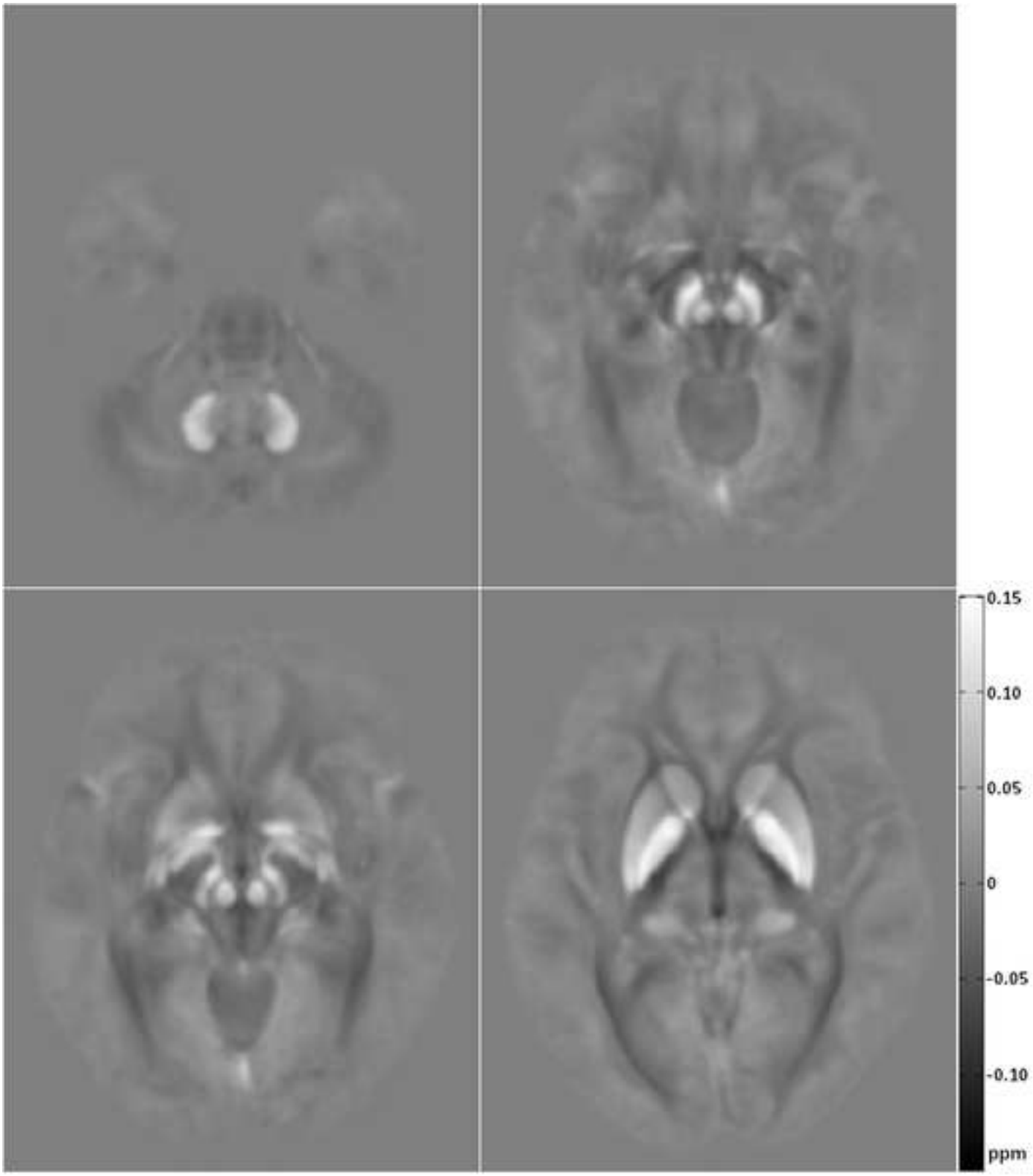

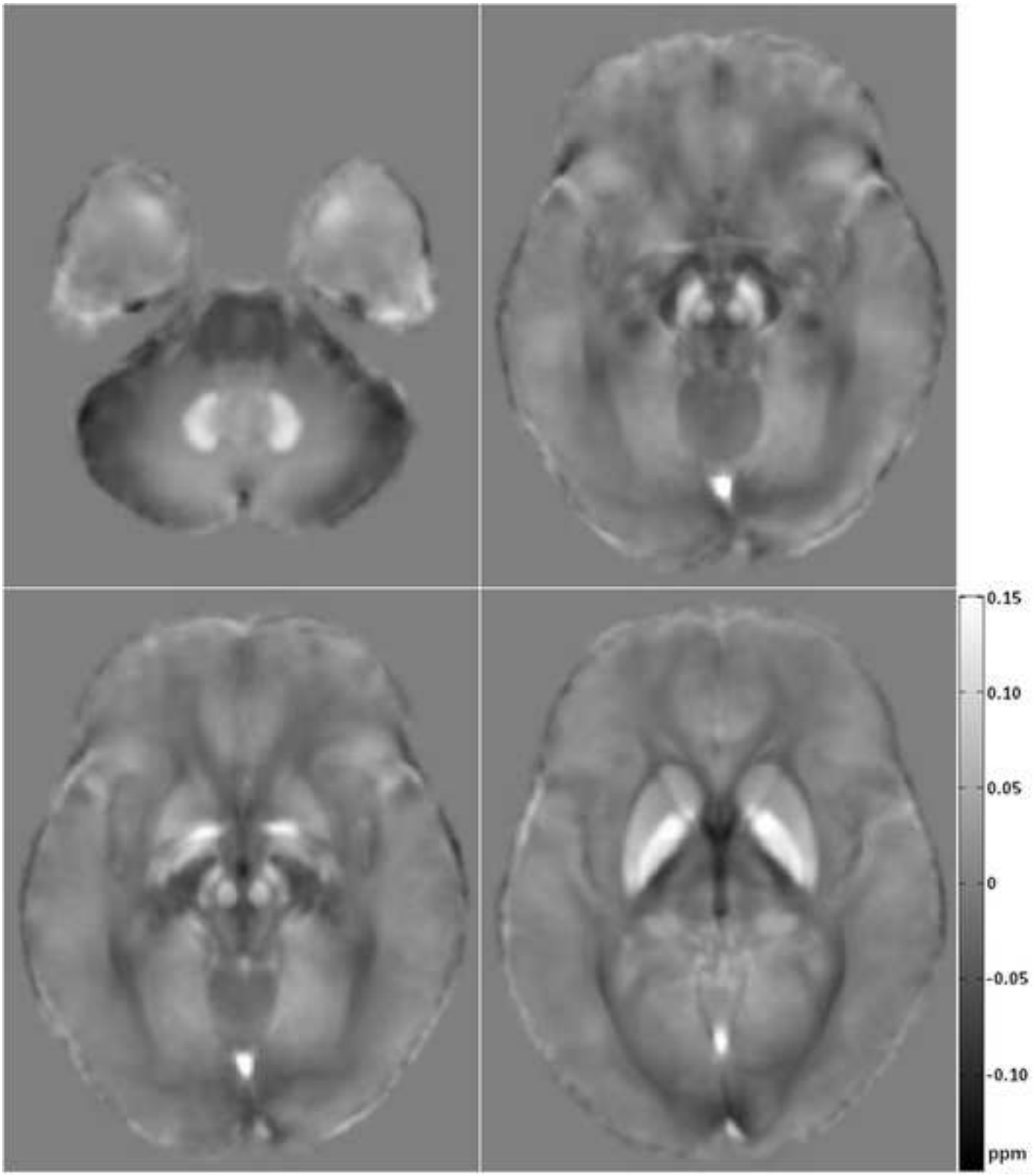

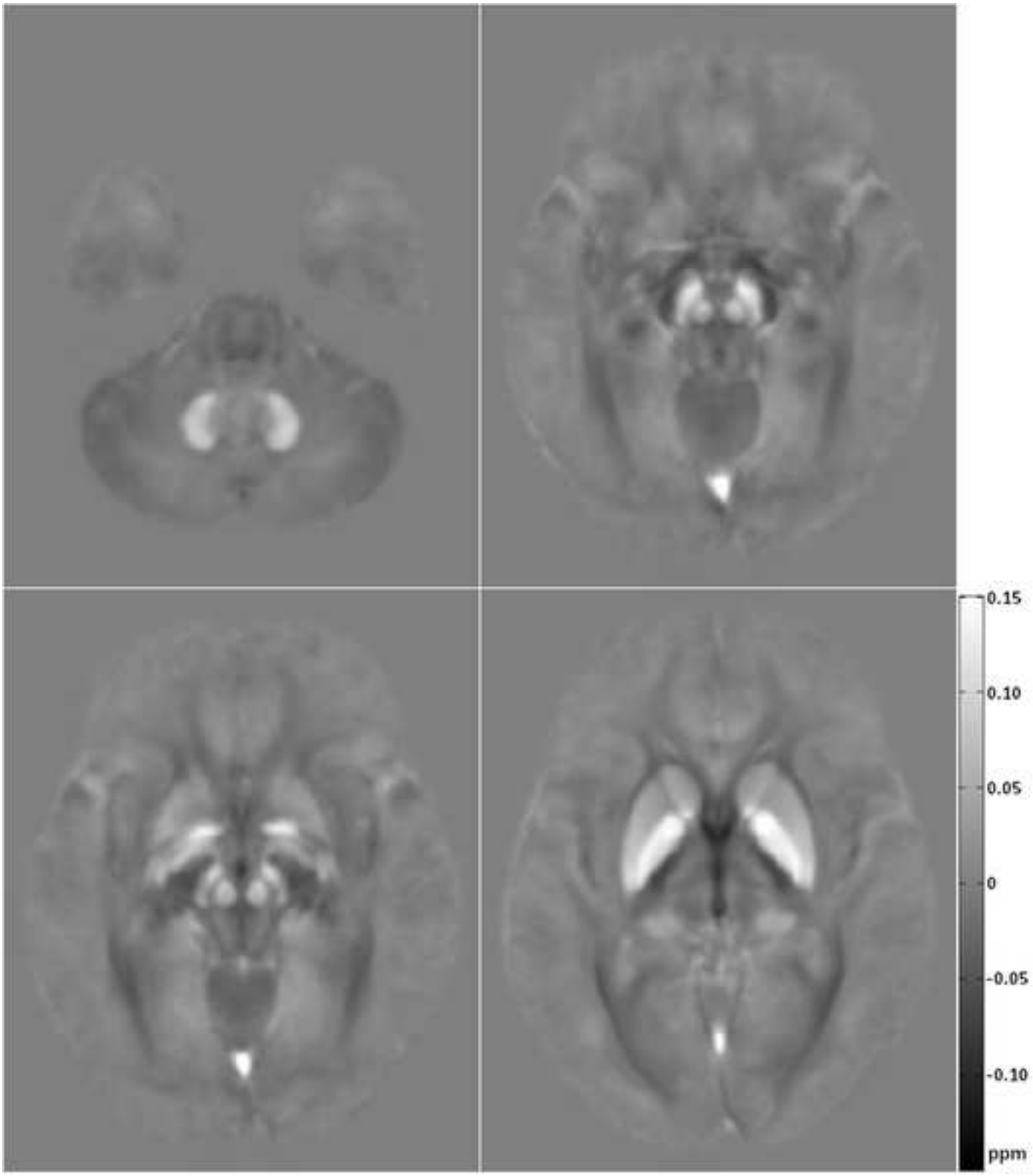

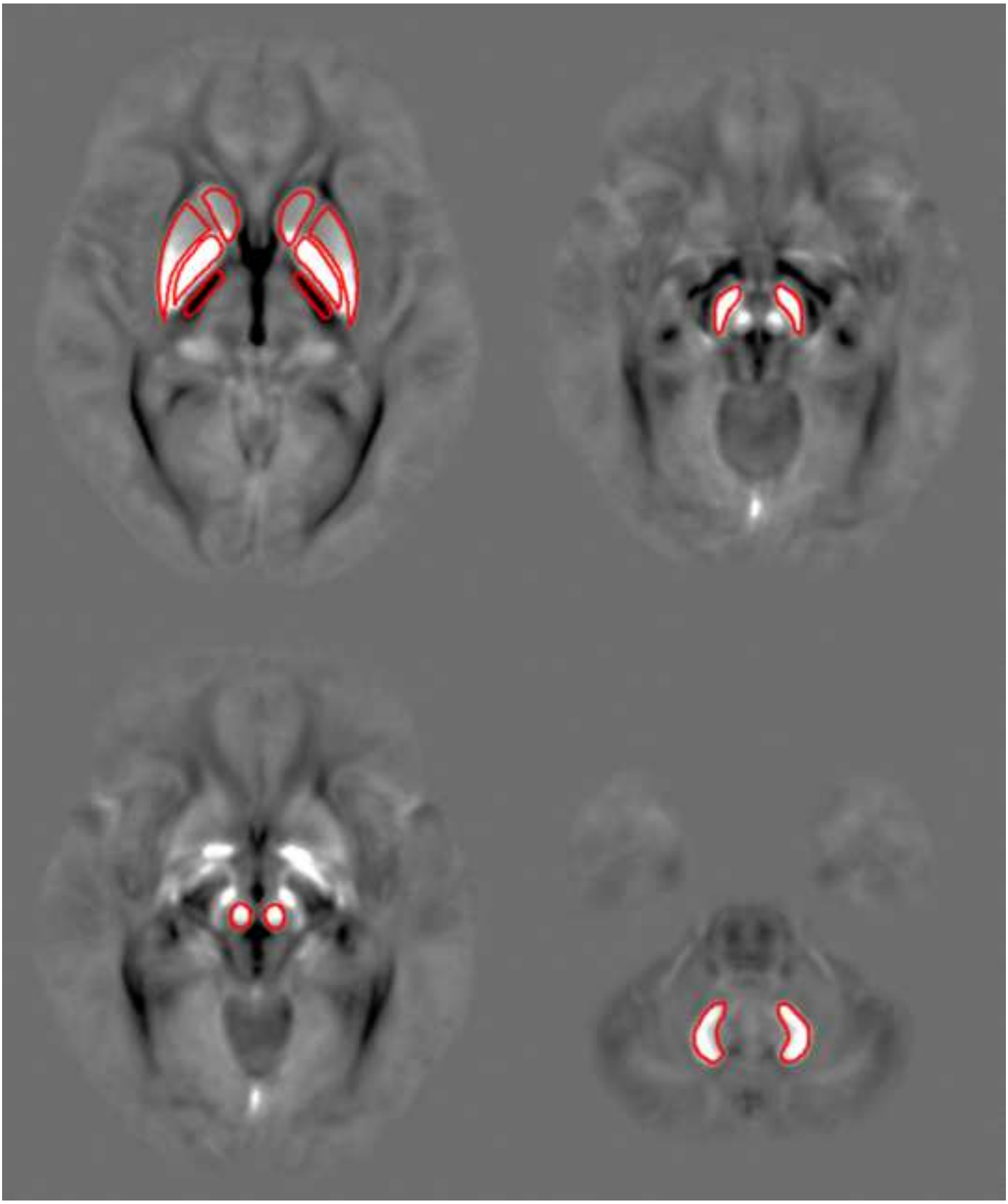

Fig.4
Click here to download high resolution image

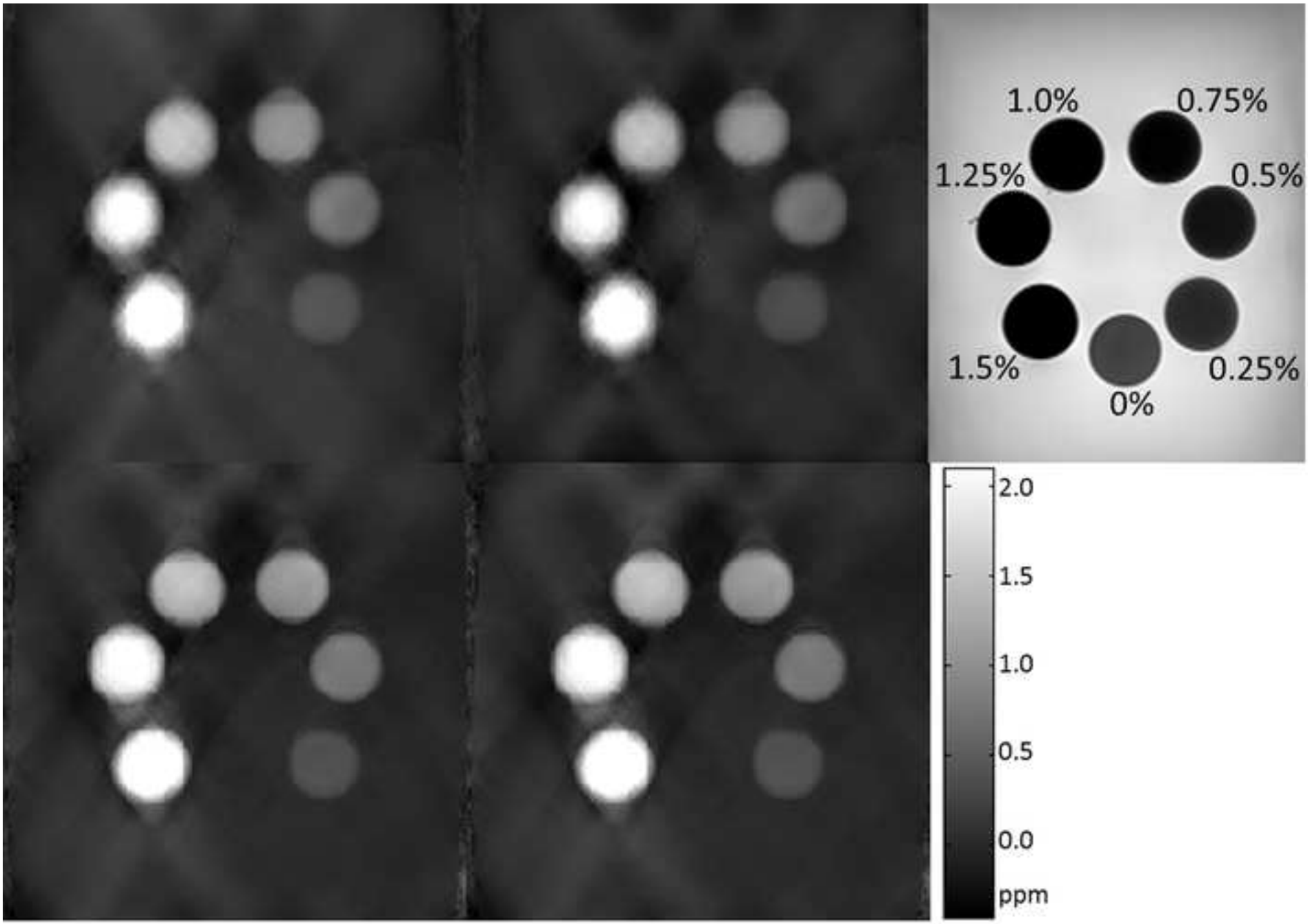

Fig.5a
Click here to download high resolution image

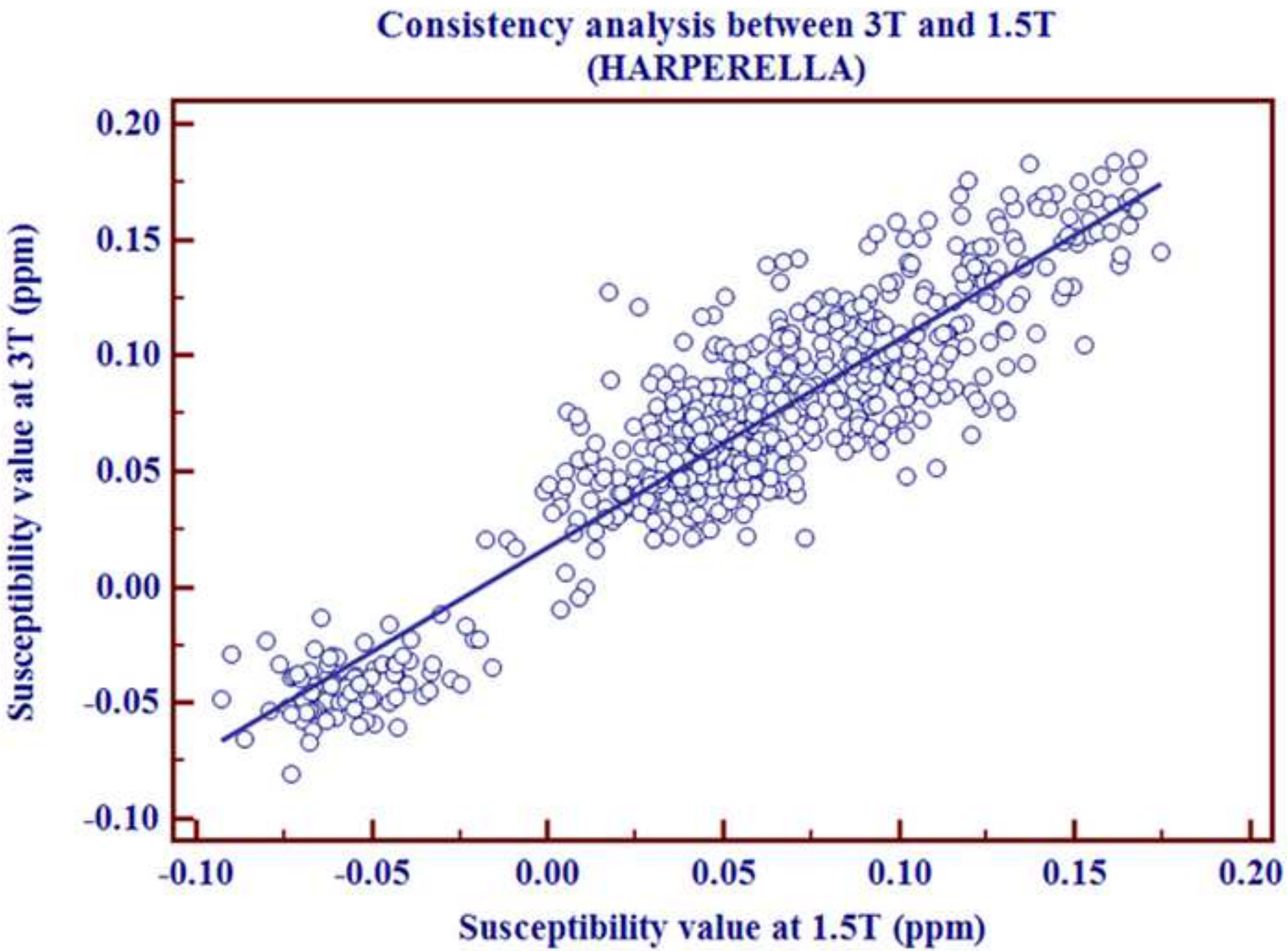

Fig.5b
Click here to download high resolution image

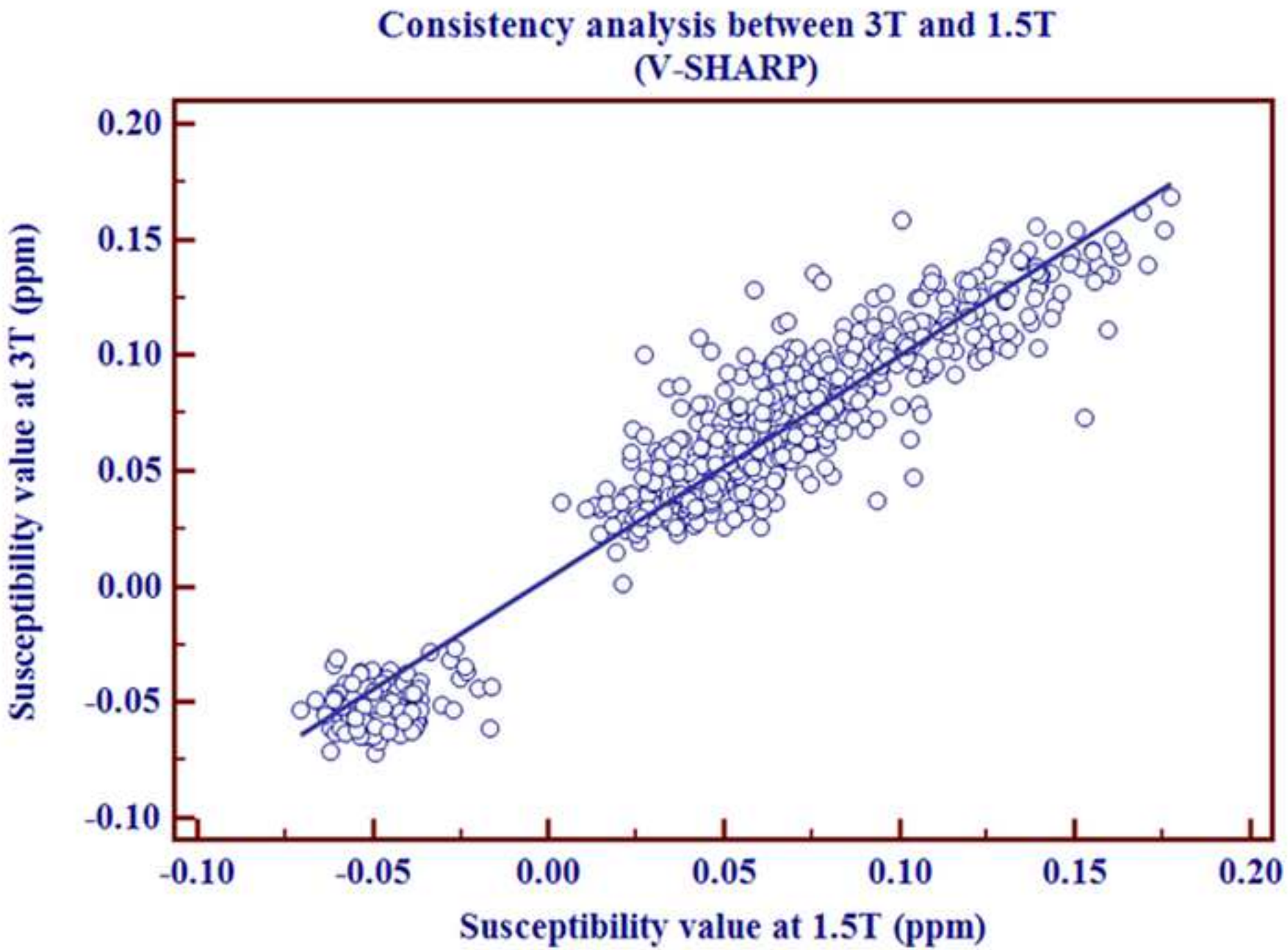

Fig.5c
Click here to download high resolution image

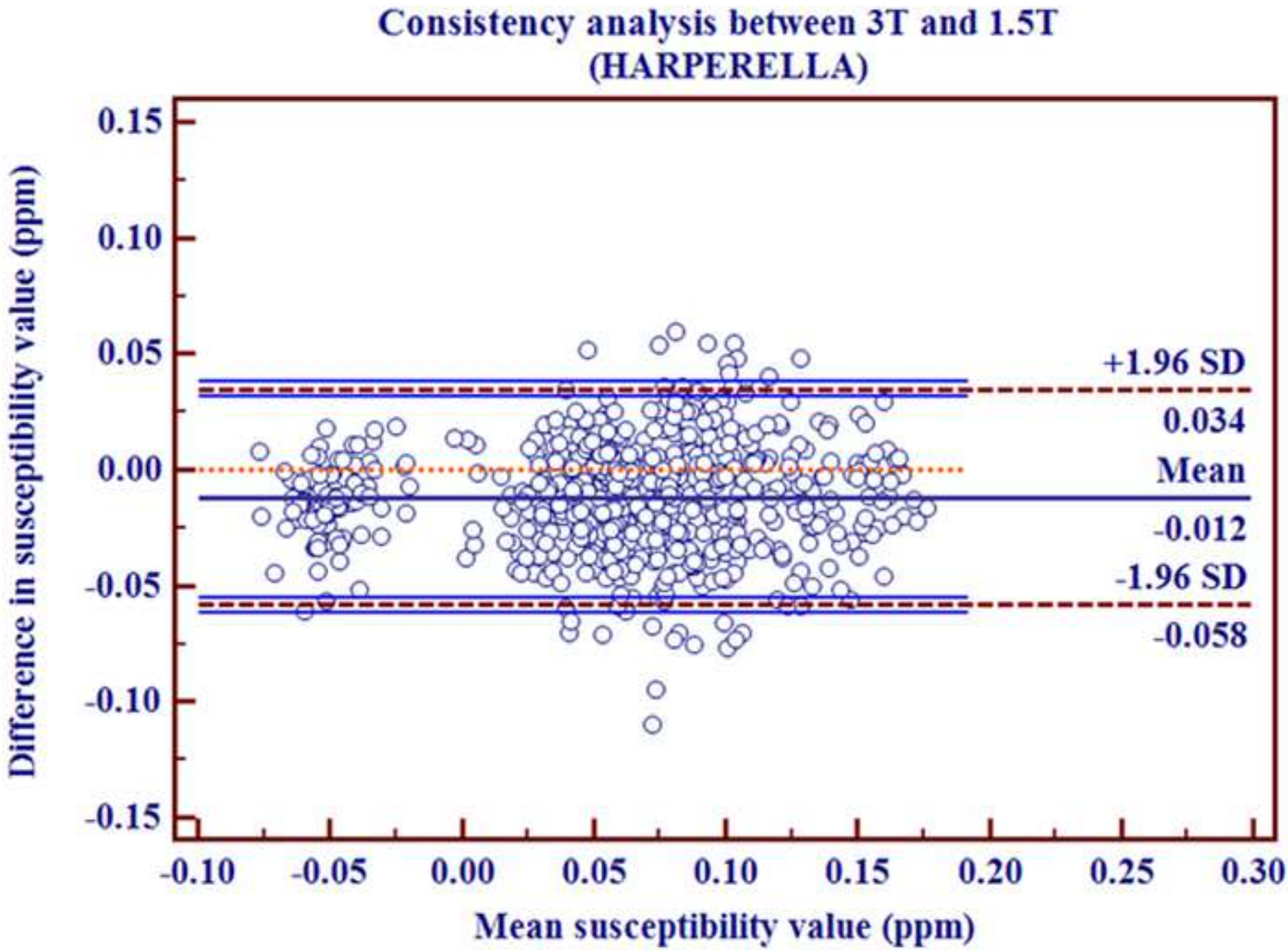

Fig.5d
Click here to download high resolution image

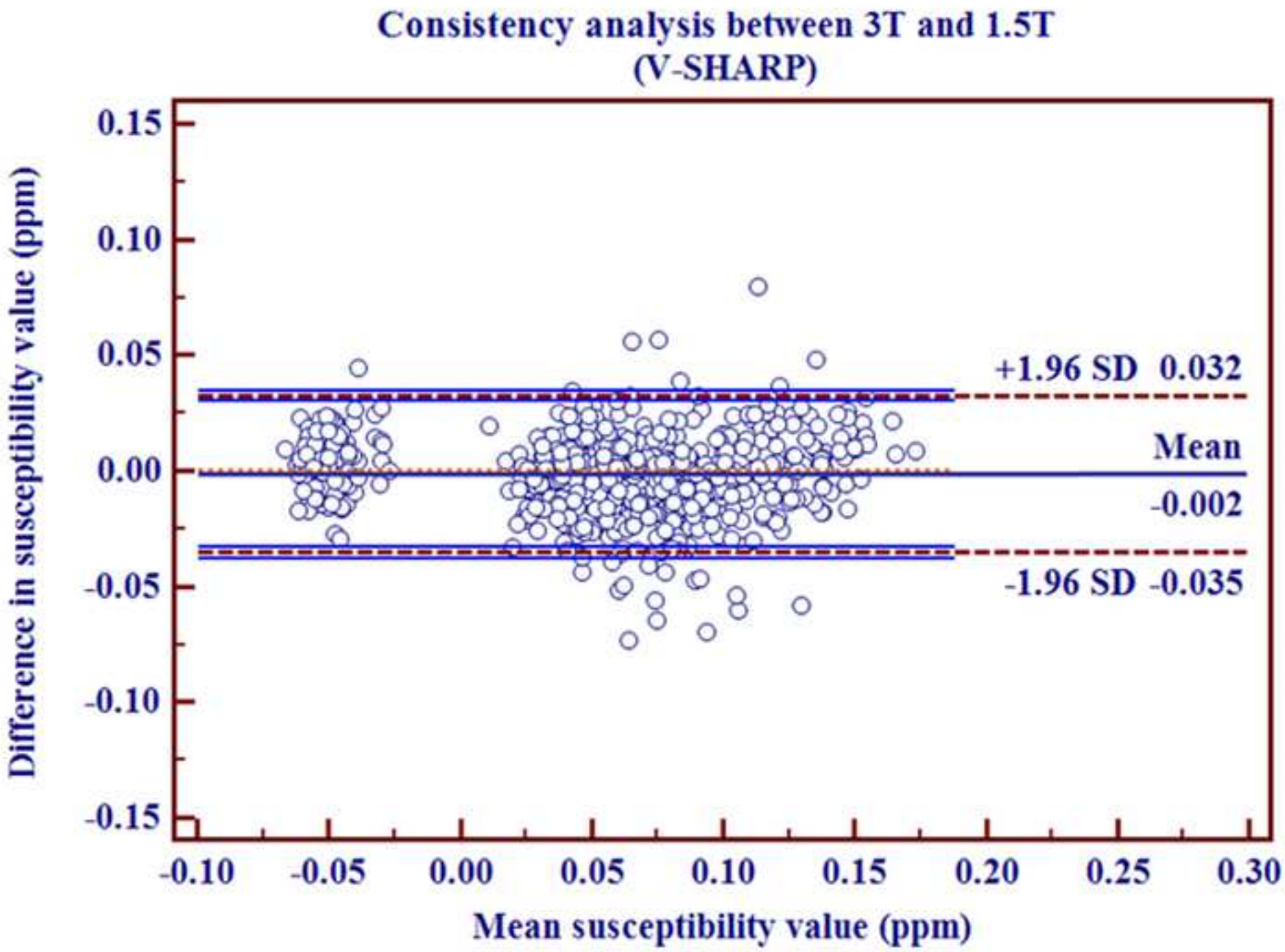

Fig.6a
Click here to download high resolution image

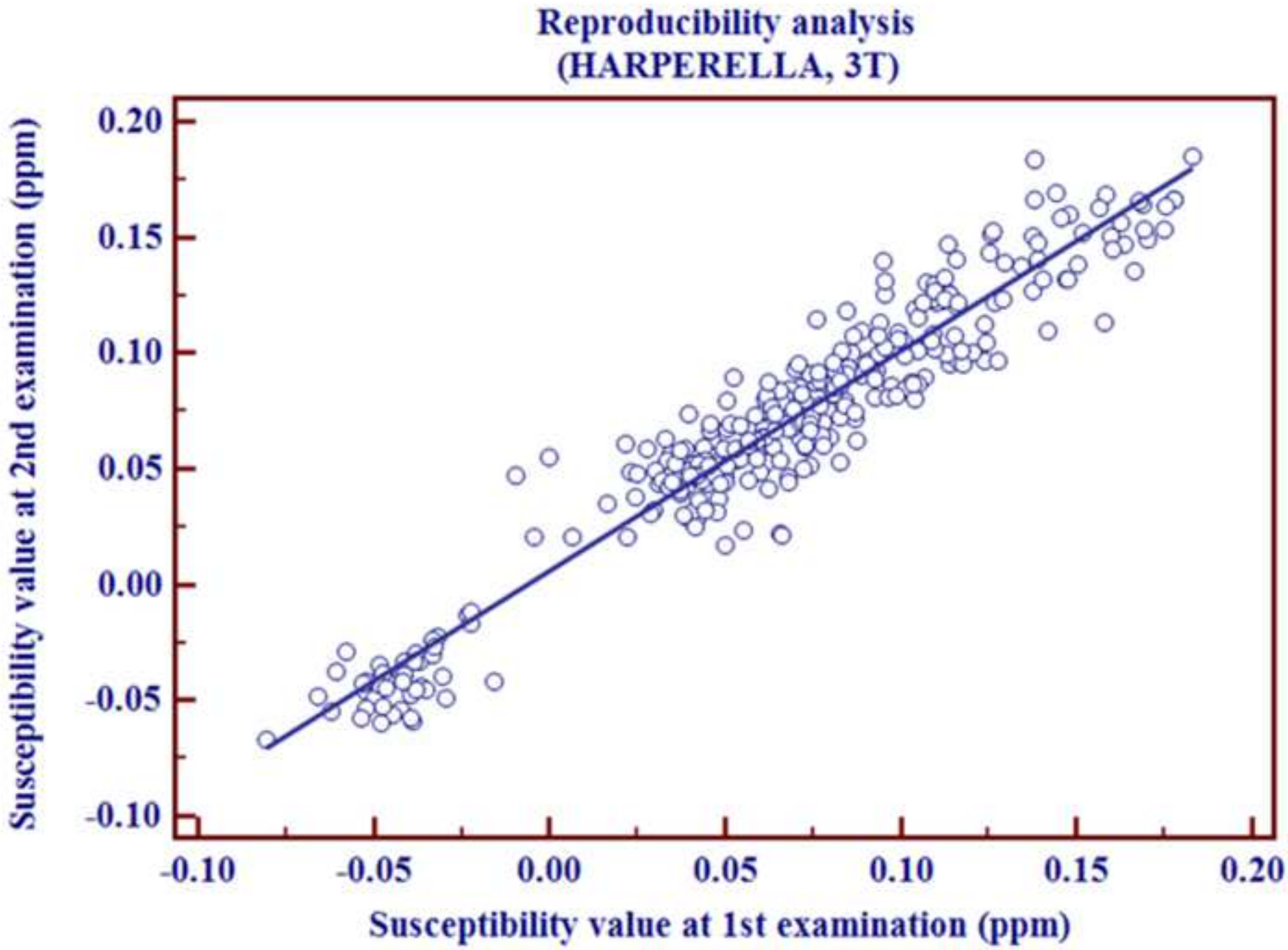

Fig.6b
Click here to download high resolution image

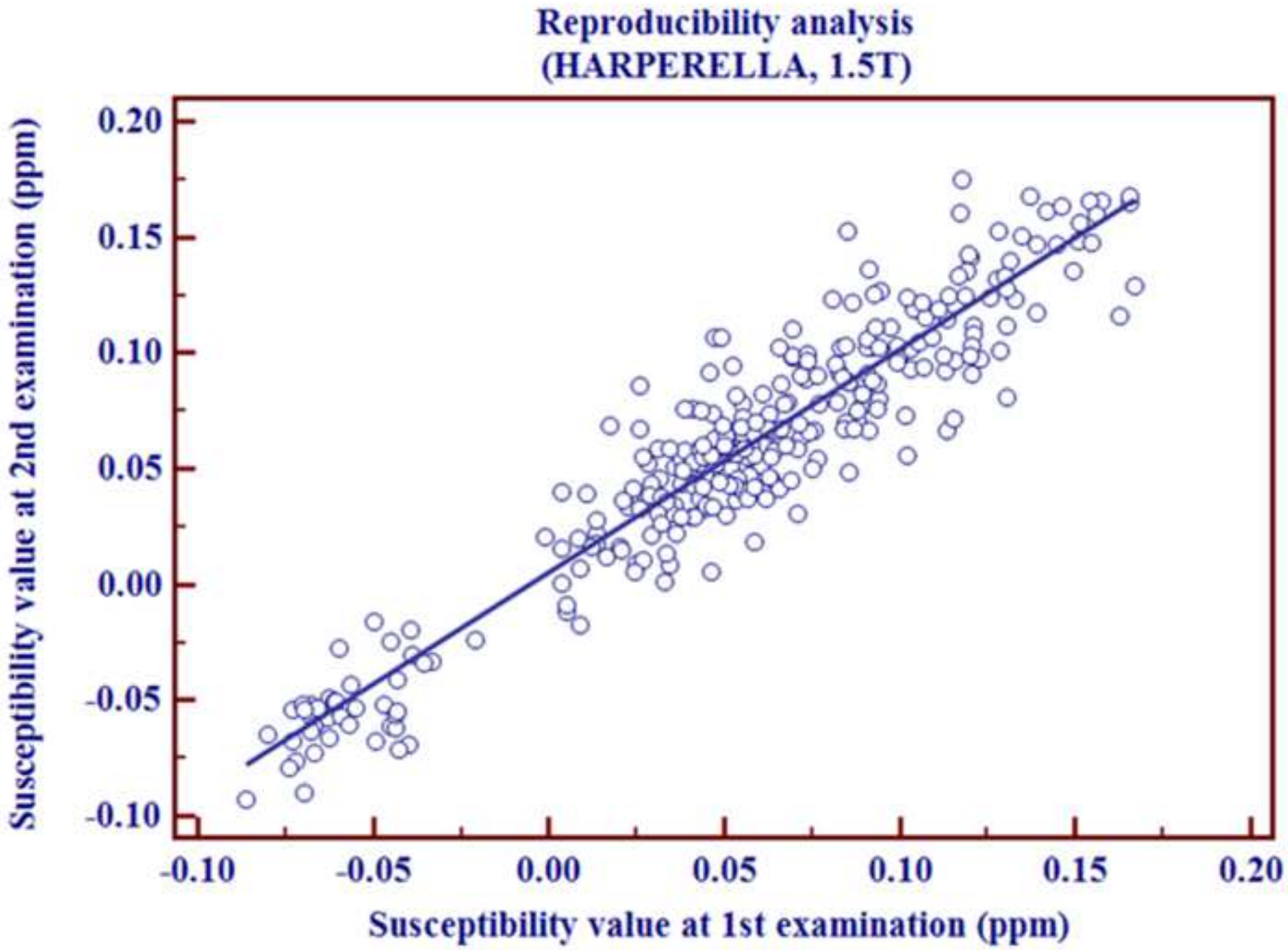

Fig.6c
Click here to download high resolution image

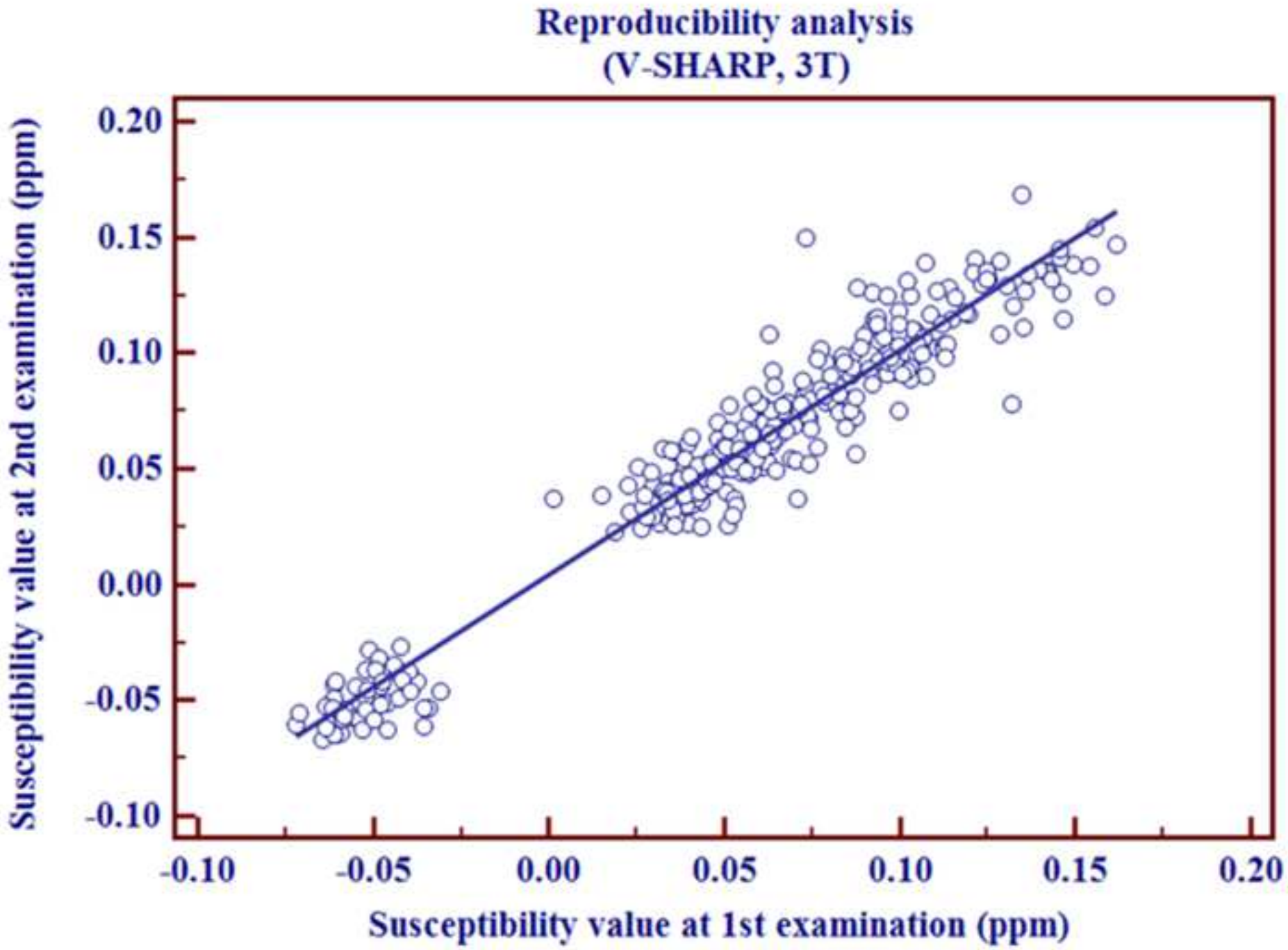

Fig.6d
Click here to download high resolution image

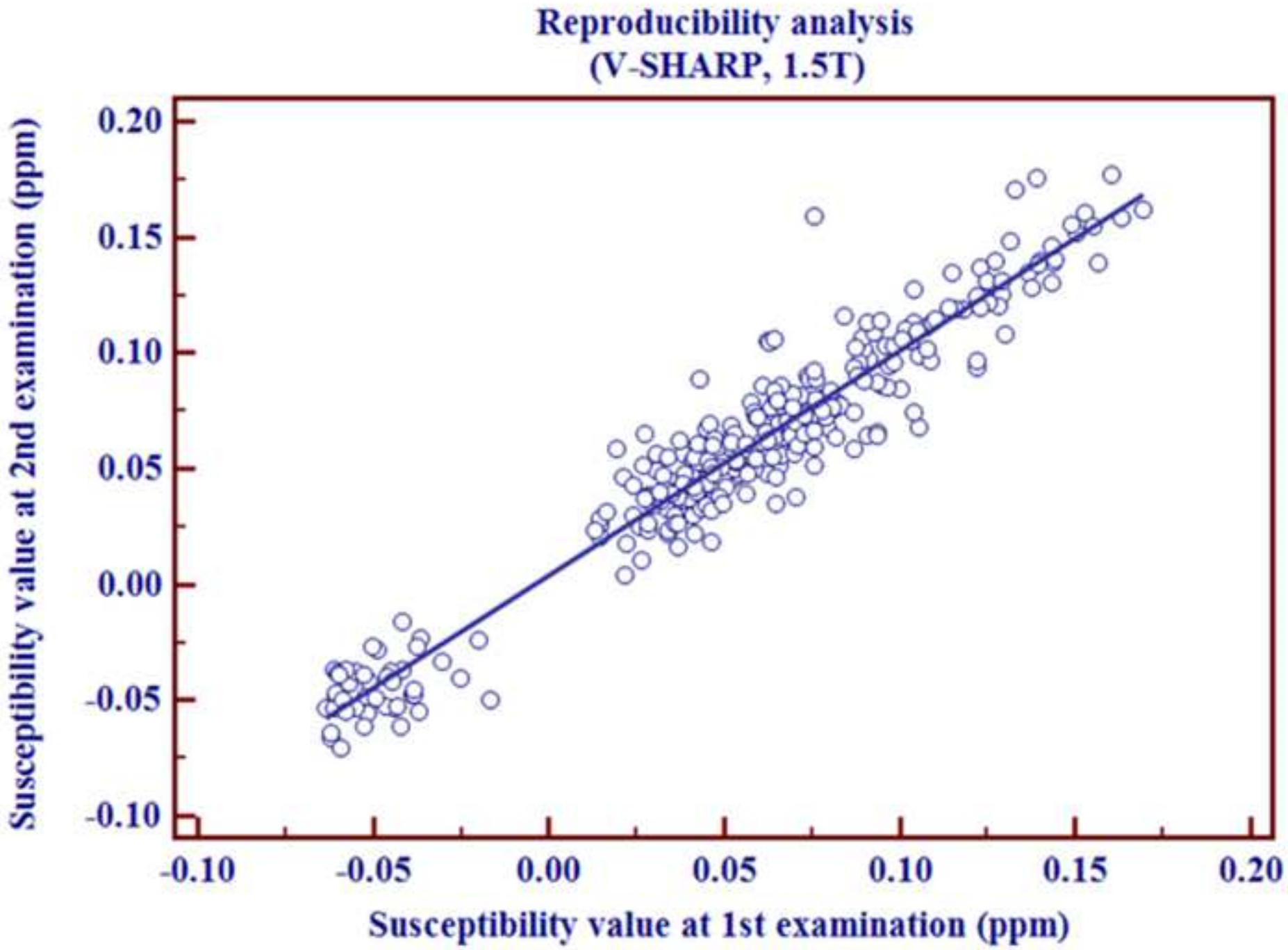

Fig.6e
Click here to download high resolution image

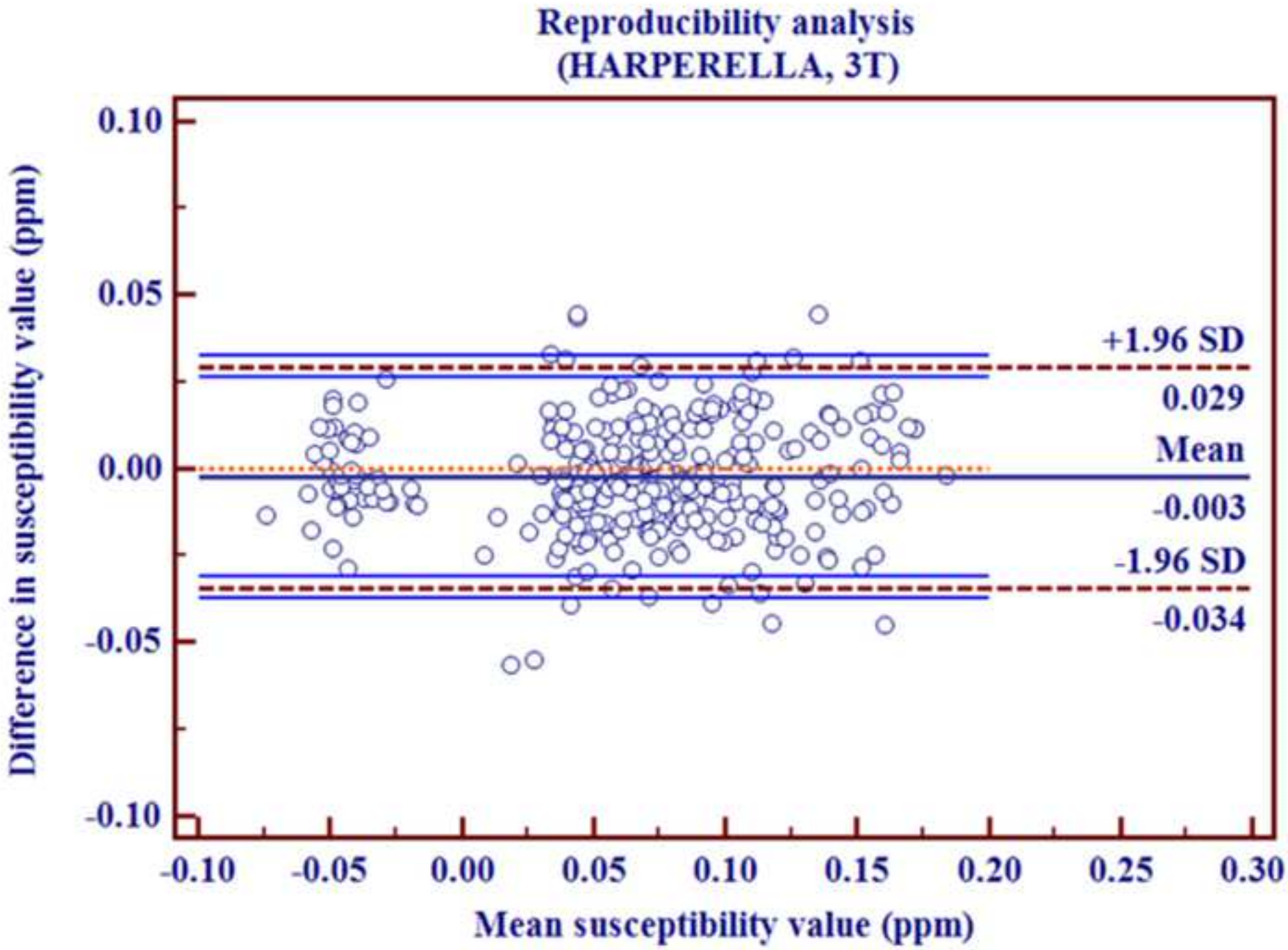

Fig.6f
Click here to download high resolution image

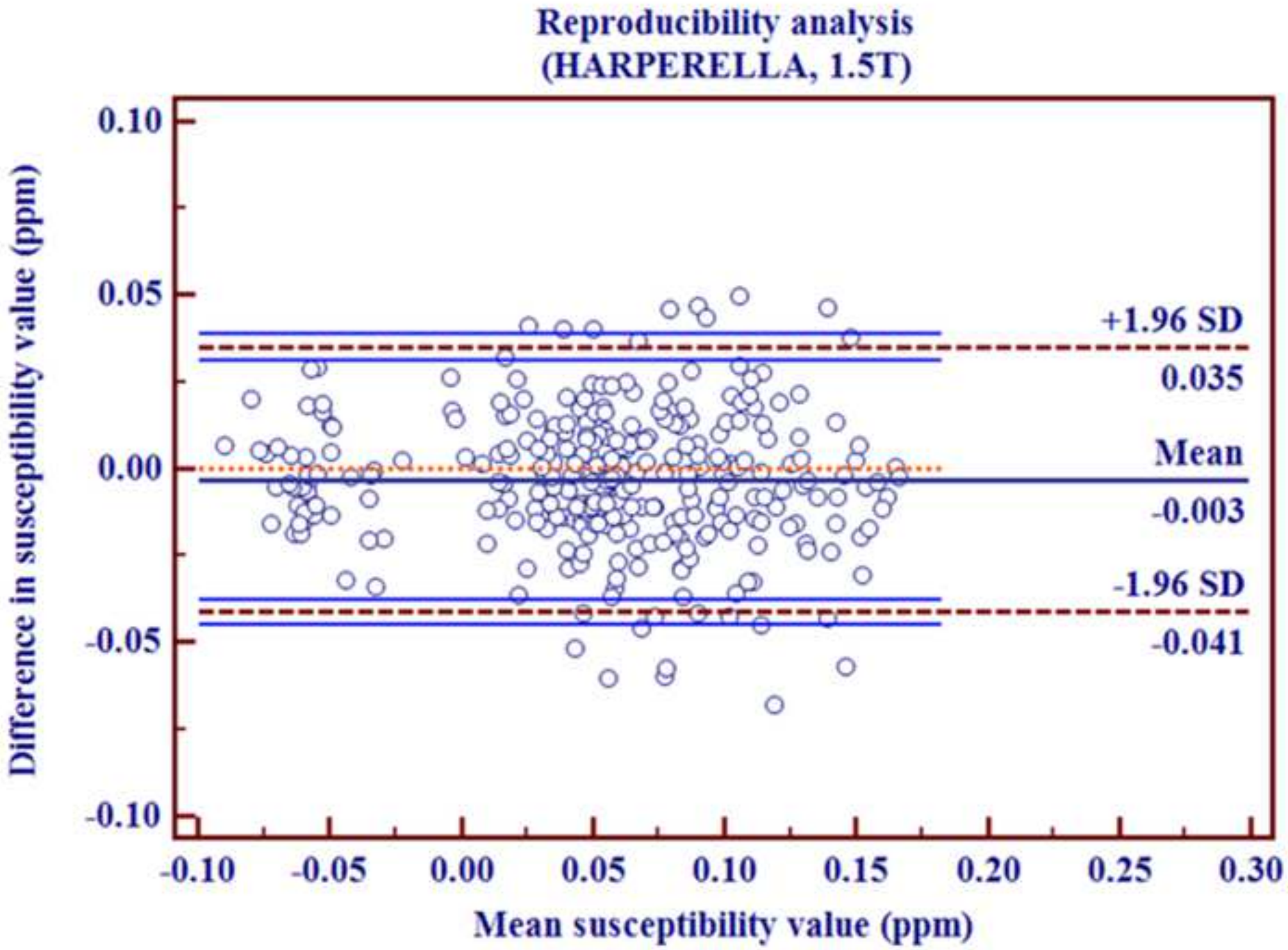

Fig.6g
Click here to download high resolution image

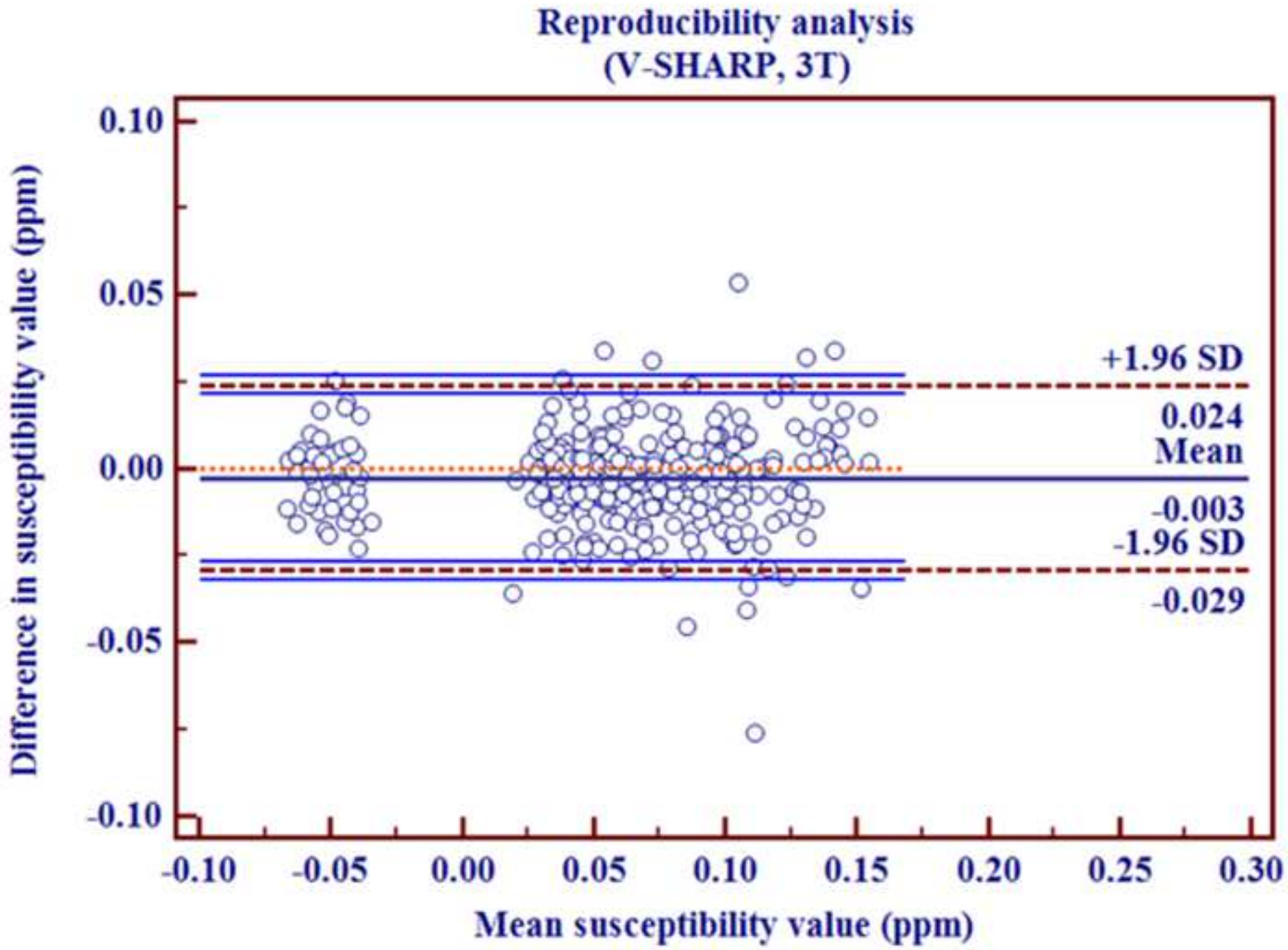

Fig.6h
Click here to download high resolution image

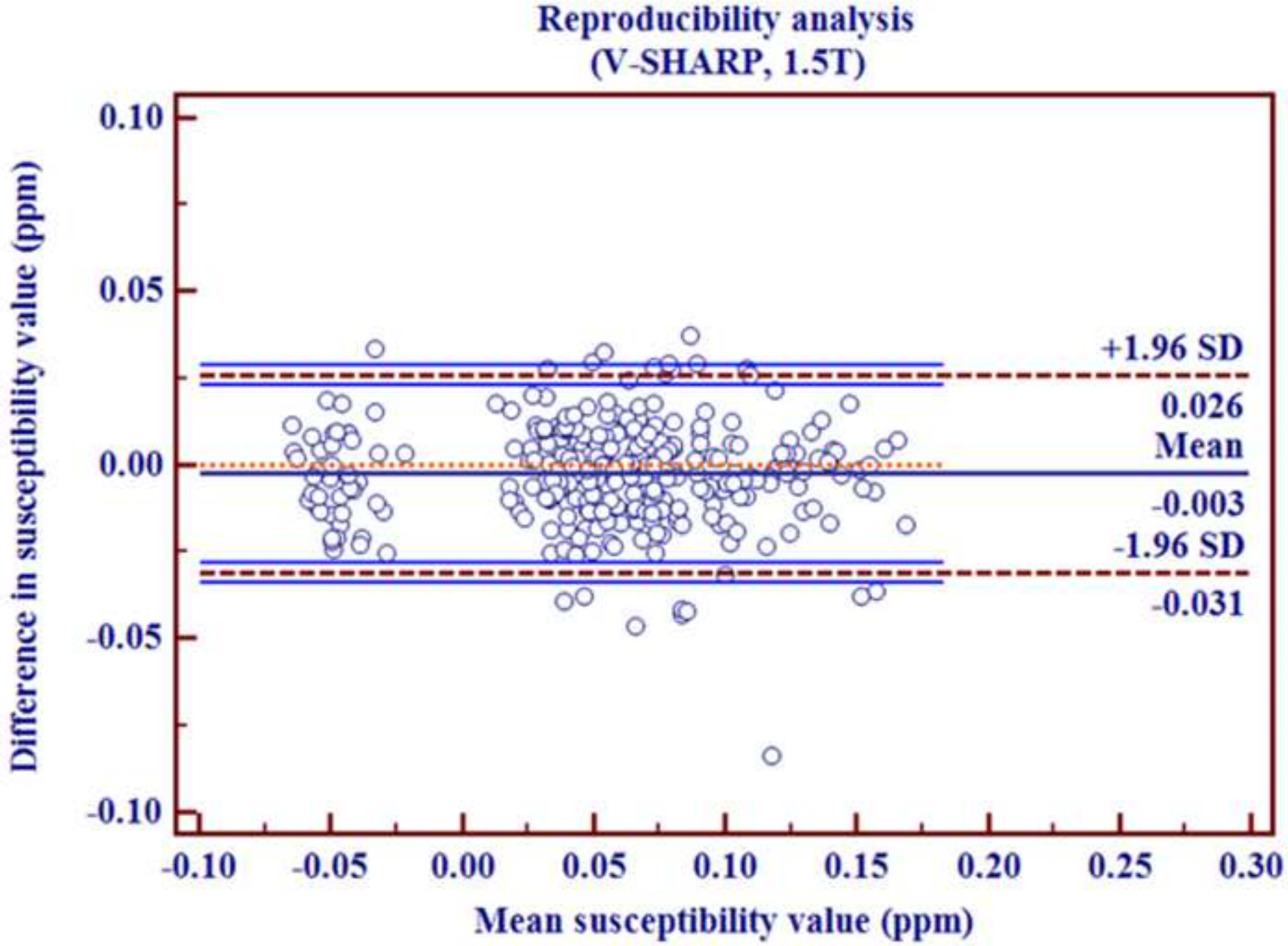

Fig.7a
Click here to download high resolution image

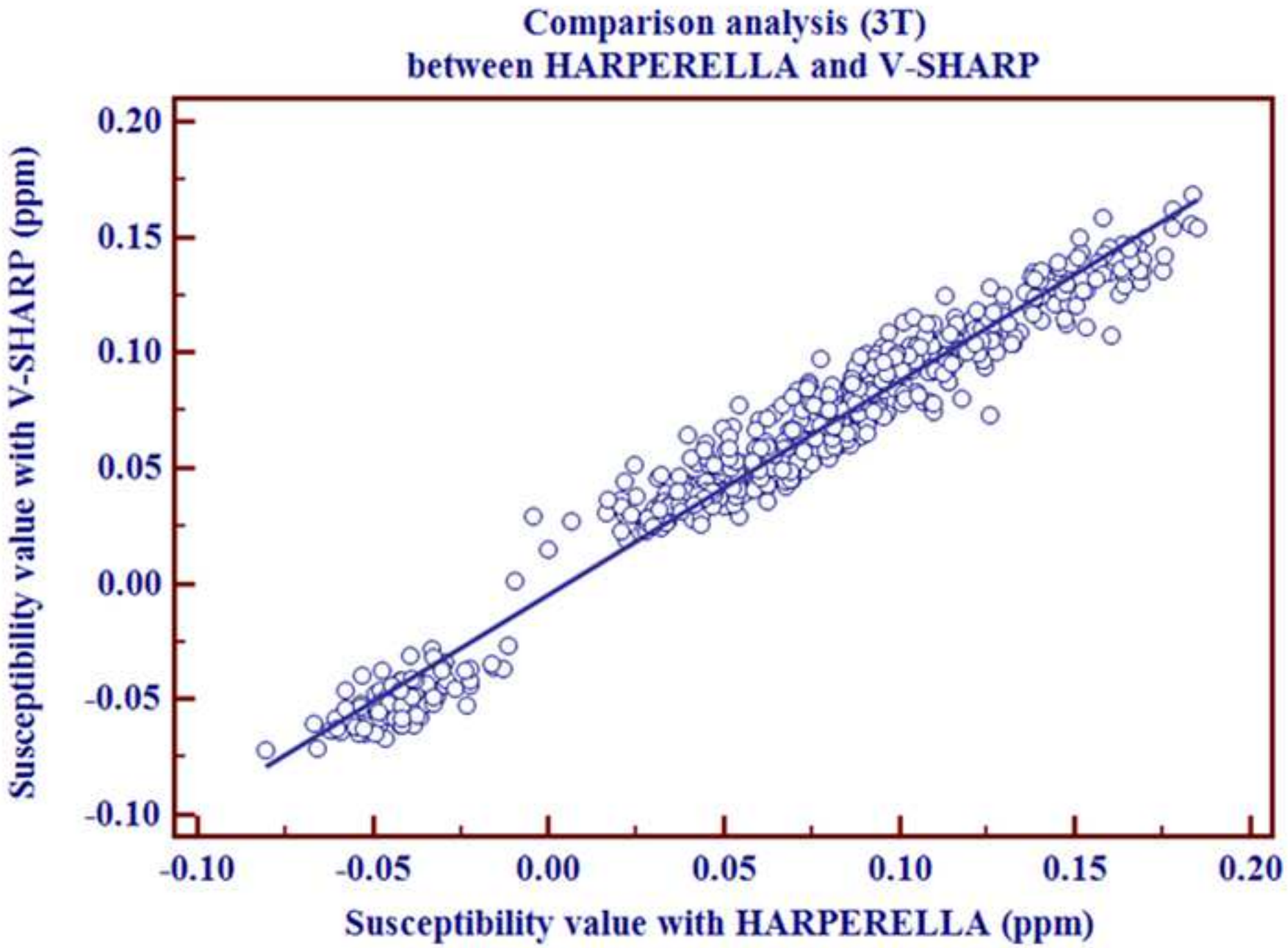

Fig.7b
Click here to download high resolution image

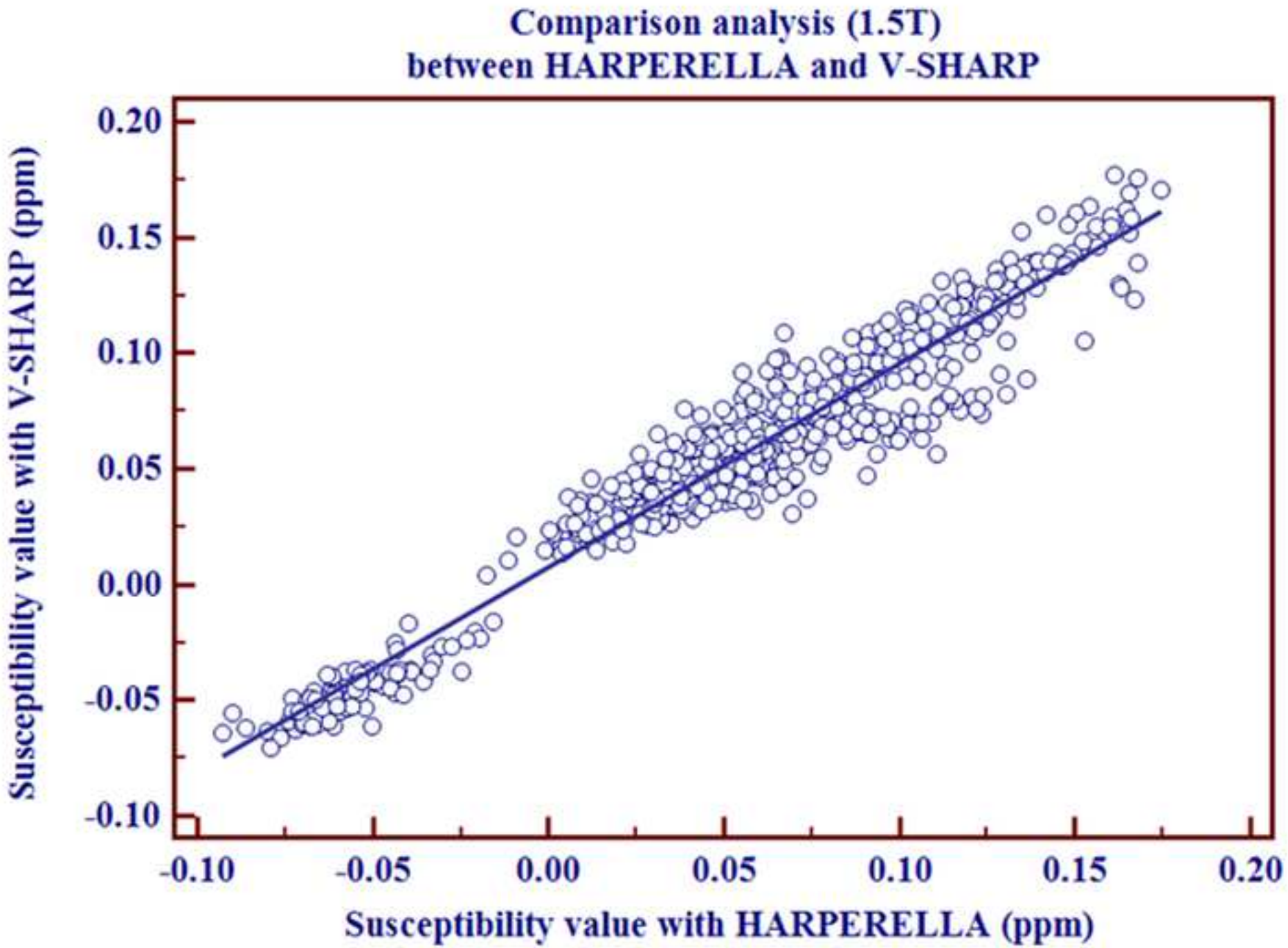

Fig.7c
Click here to download high resolution image

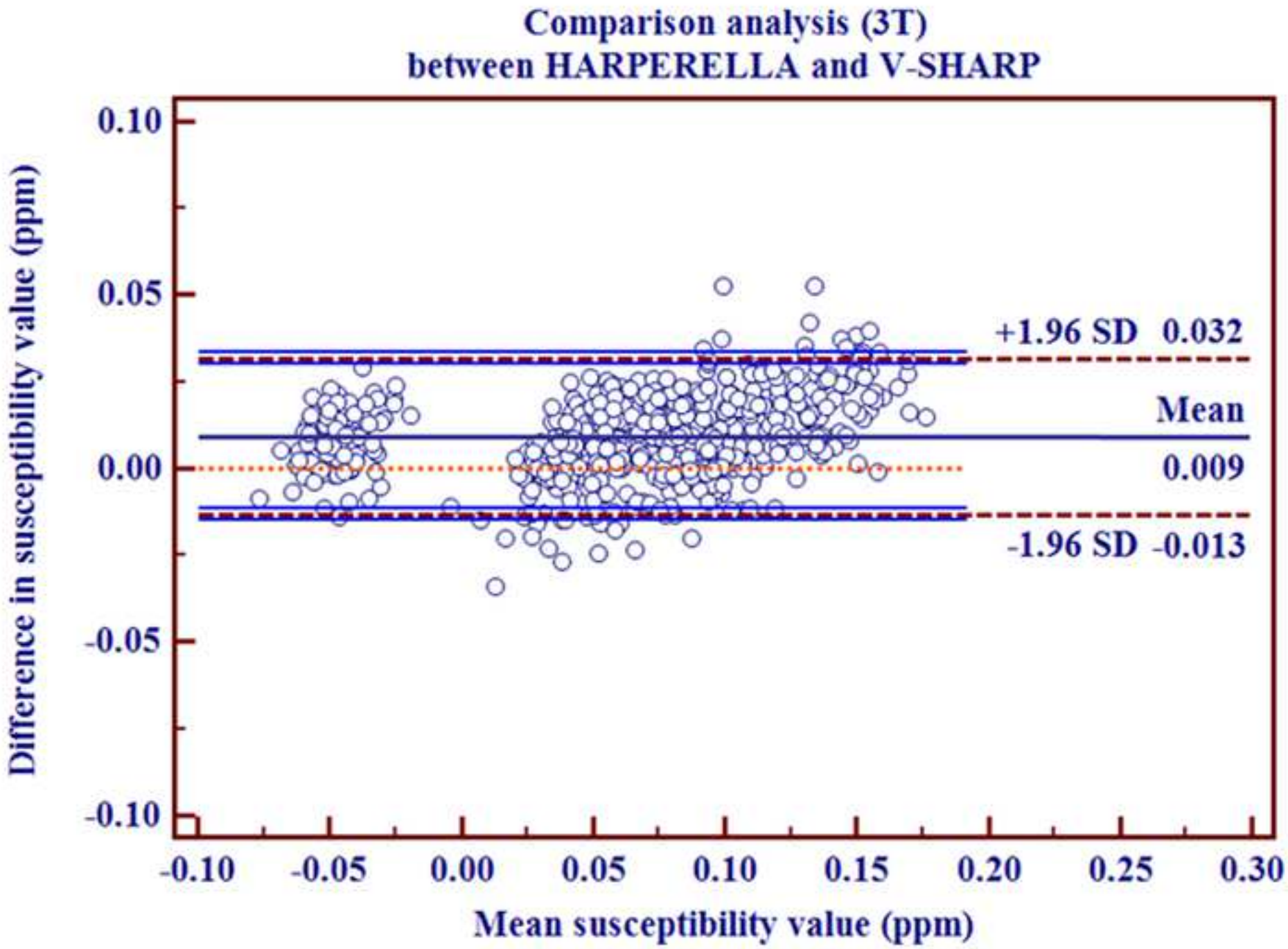

Fig.7d
Click here to download high resolution image

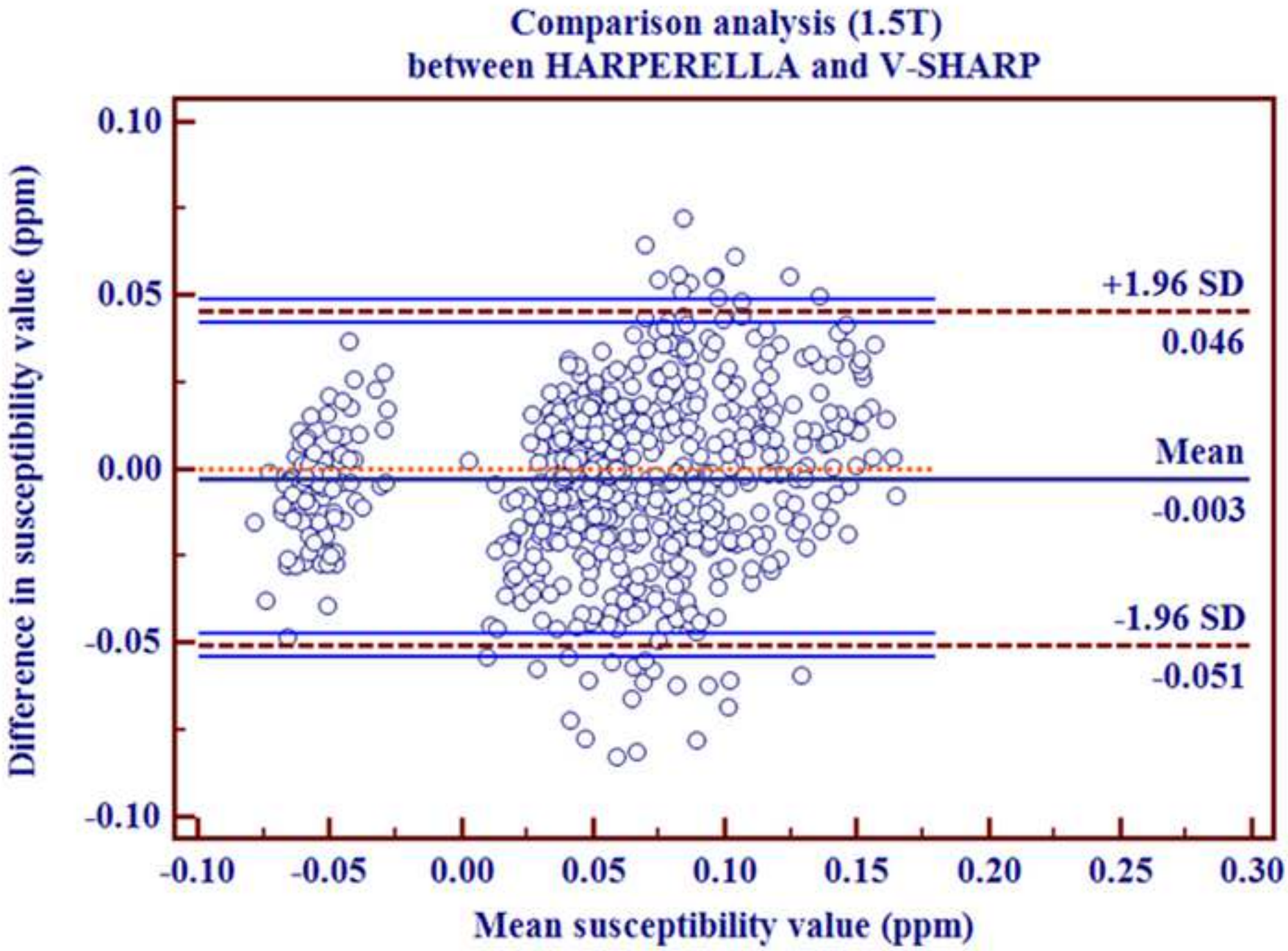

Supplemental Digital Content 1

Scattered plots of the region of interest analysis. Scattered plots show linear regression analysis with theoretical susceptibility values of (a) measured susceptibility values at 3T with HARPERELLA, (b) with V-SHARP, (c) at 1.5T with HARPERELLA, and (d) with V-SHARP. Linear regression analysis between 3T and 1.5T (e) with HARPERELLA and (f) V-SHARP.

Supplemental Digital Content 2

Mean susceptibility values by the single set of ROIs and each rater on (a) QSM with HARPERELLA at 3T, (b) with V-SHARP at 3T, (c) with HARPERELLA at 1.5T and (d) with V-SHARP at 1.5T.

Supplemental Digital Content 1 (a)

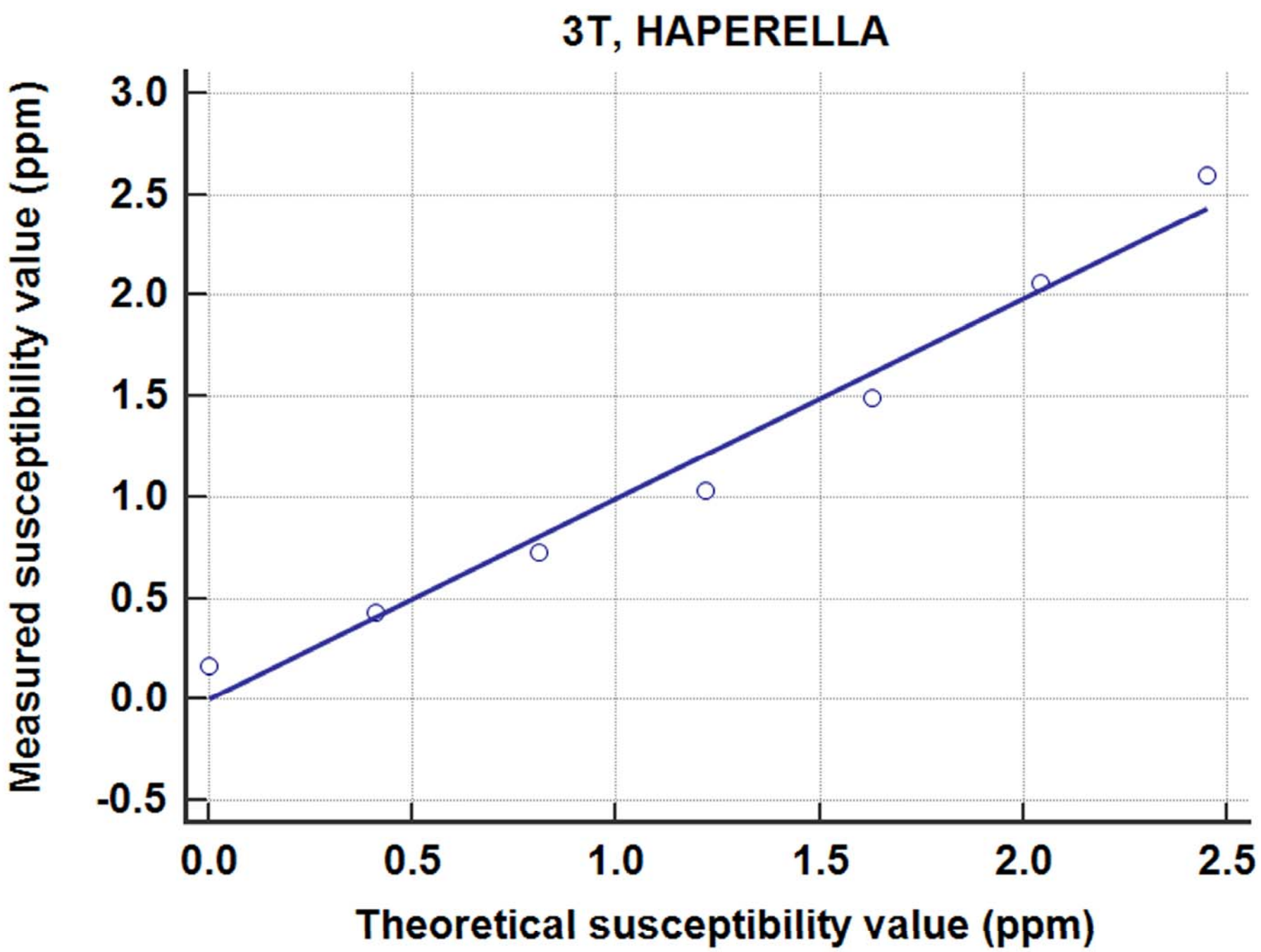

Supplemental Digital Content 1 (b)

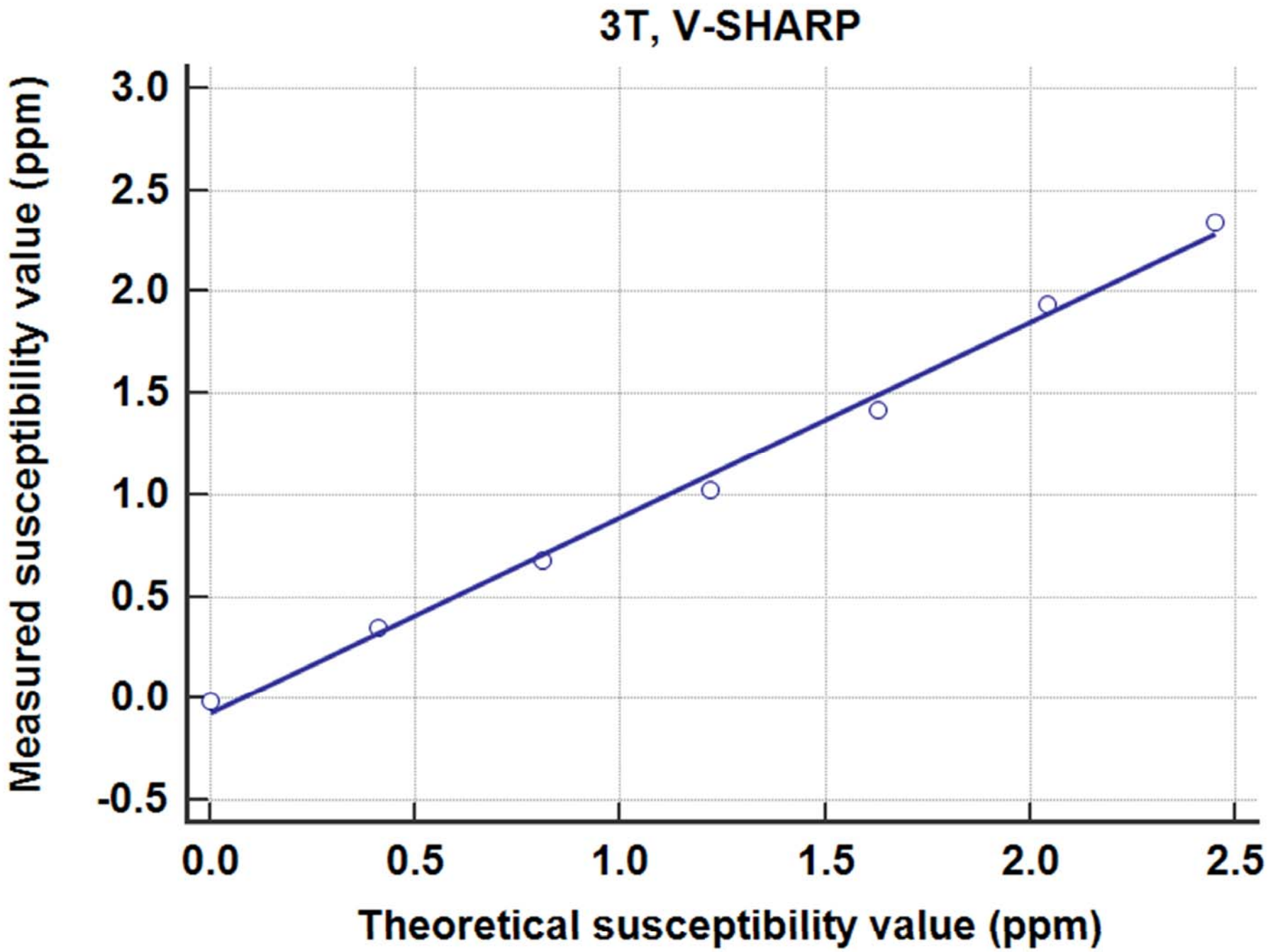

Supplemental Digital Content 1 (c)

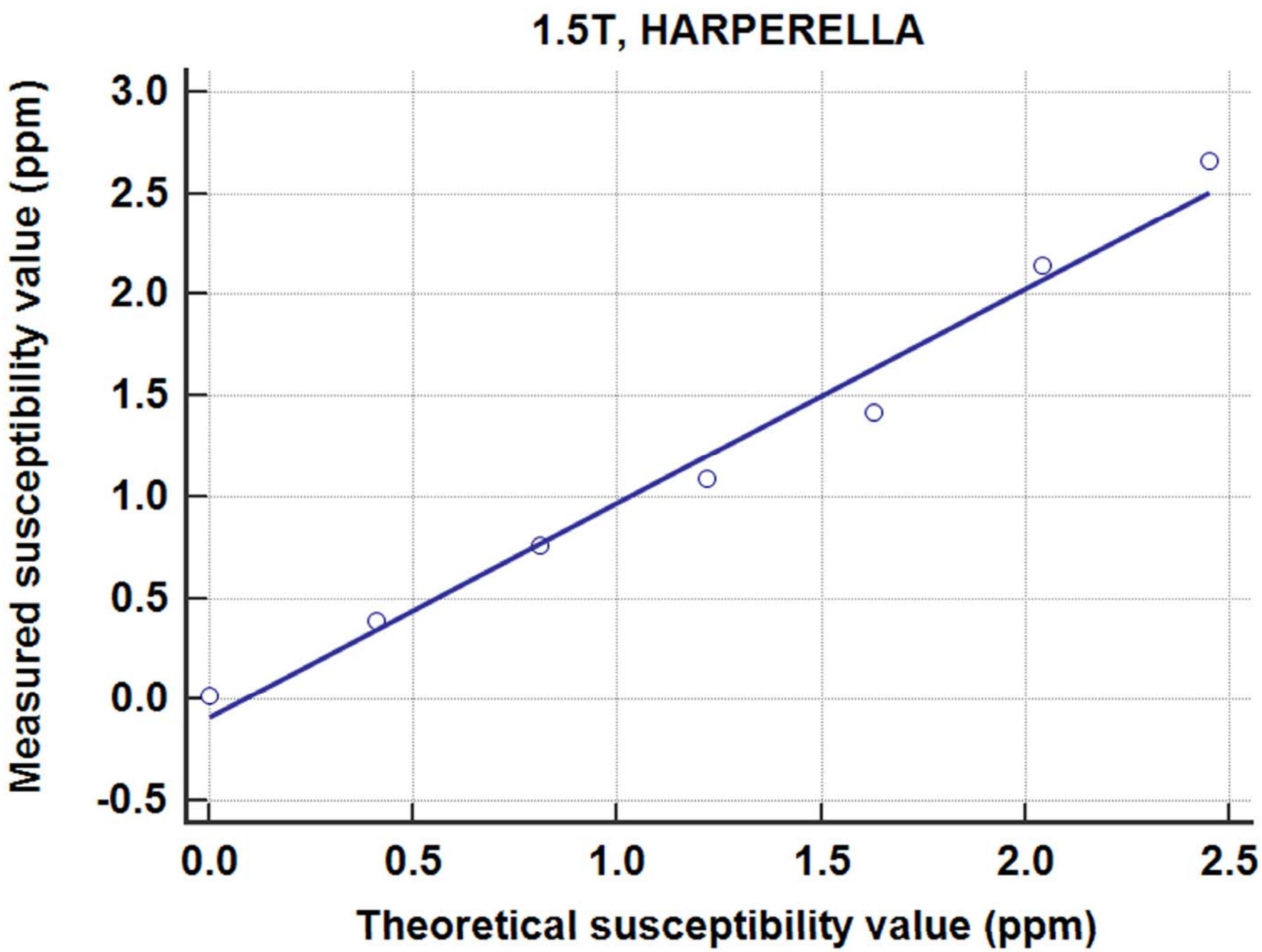

Supplemental Digital Content 1 (d)

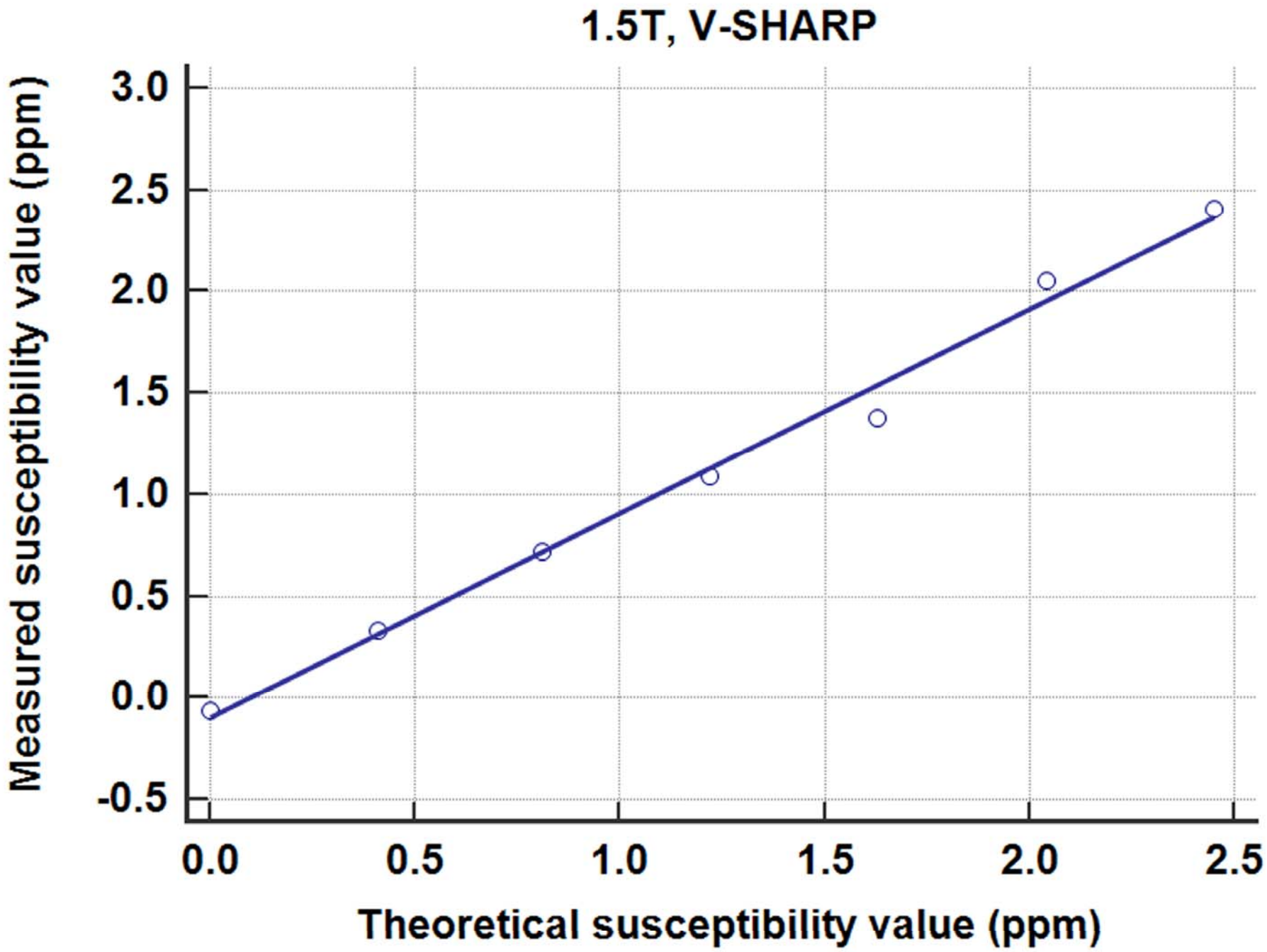

Supplemental Digital Content 1 (e)

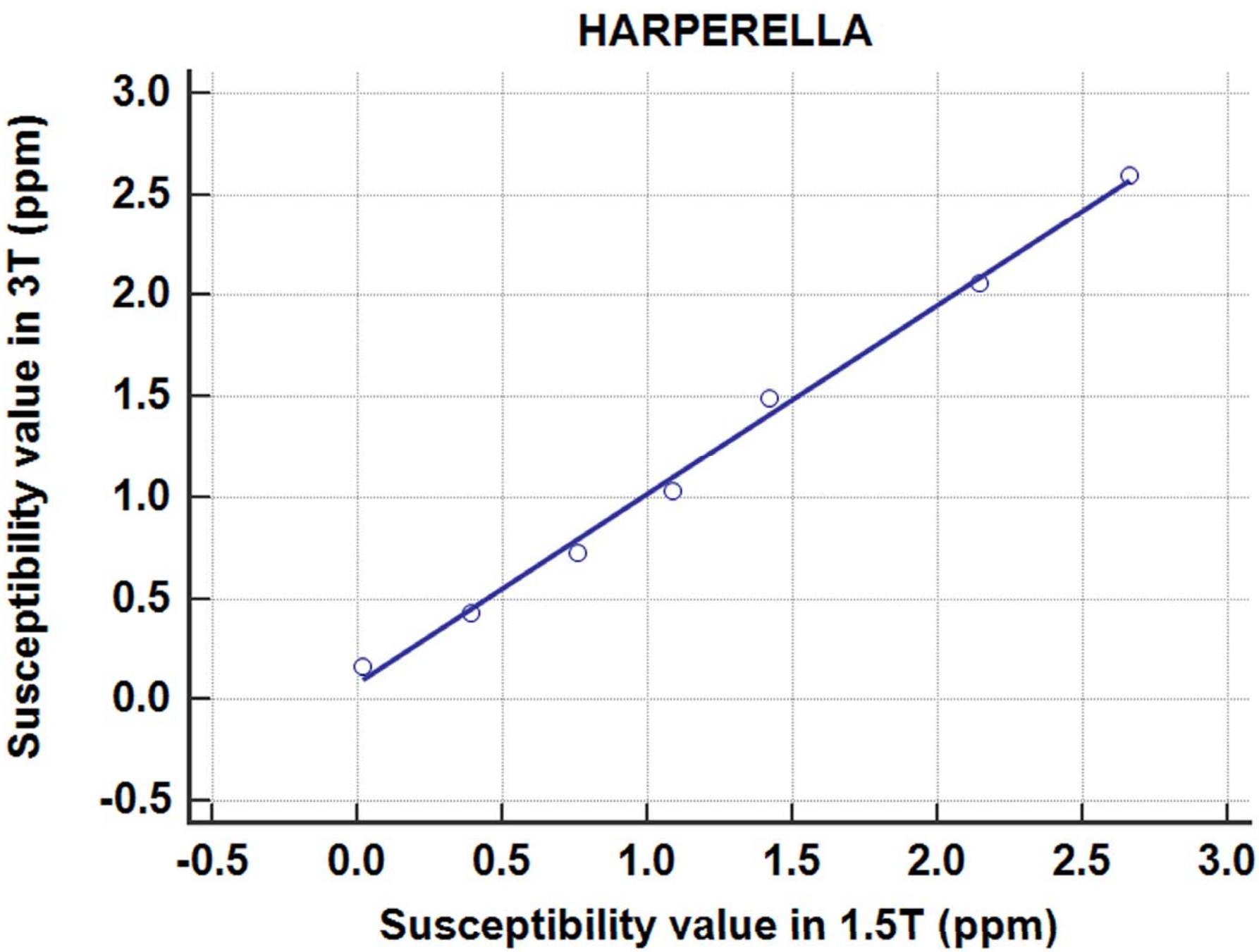

Supplemental Digital Content 1 (f)

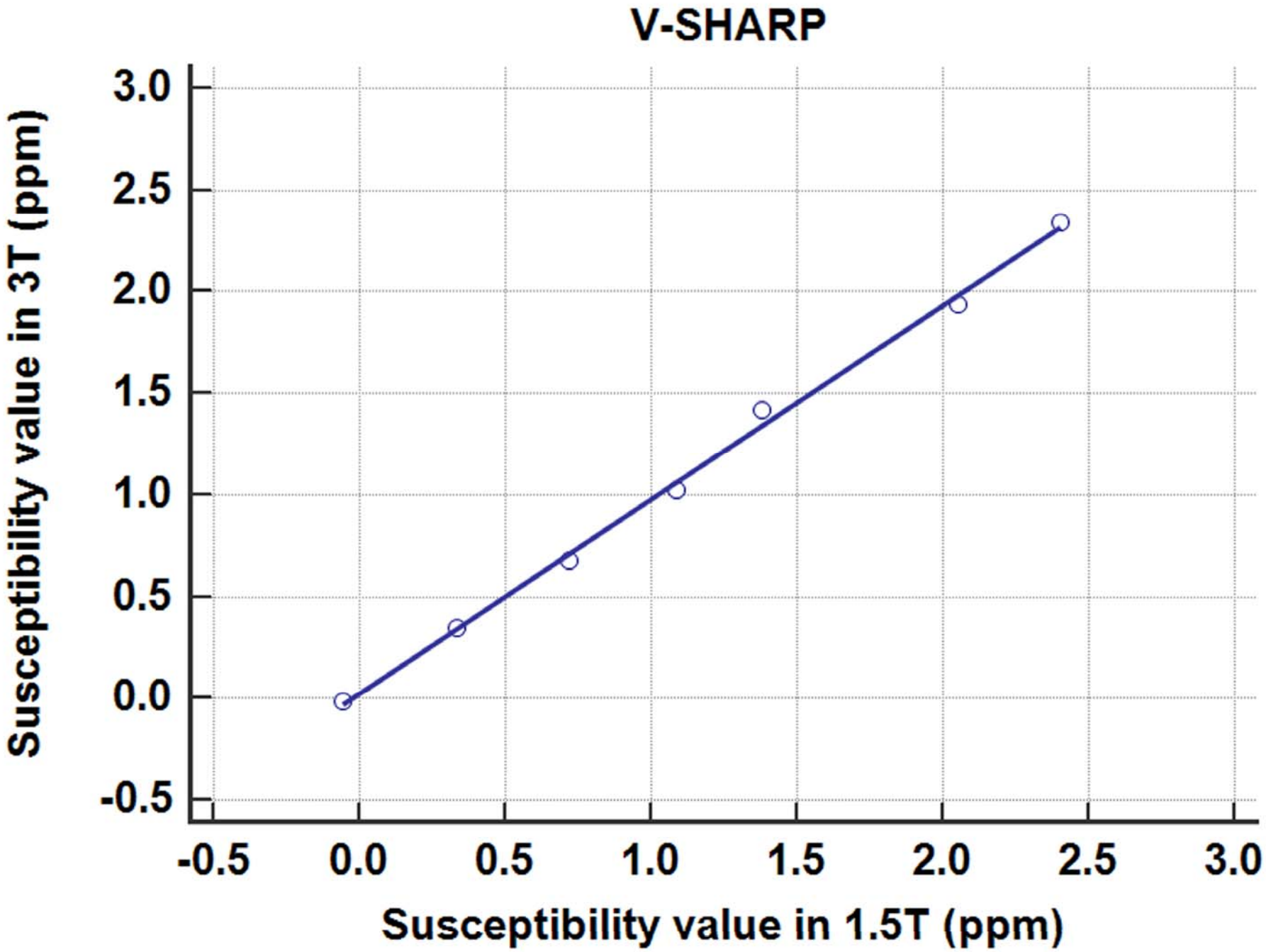

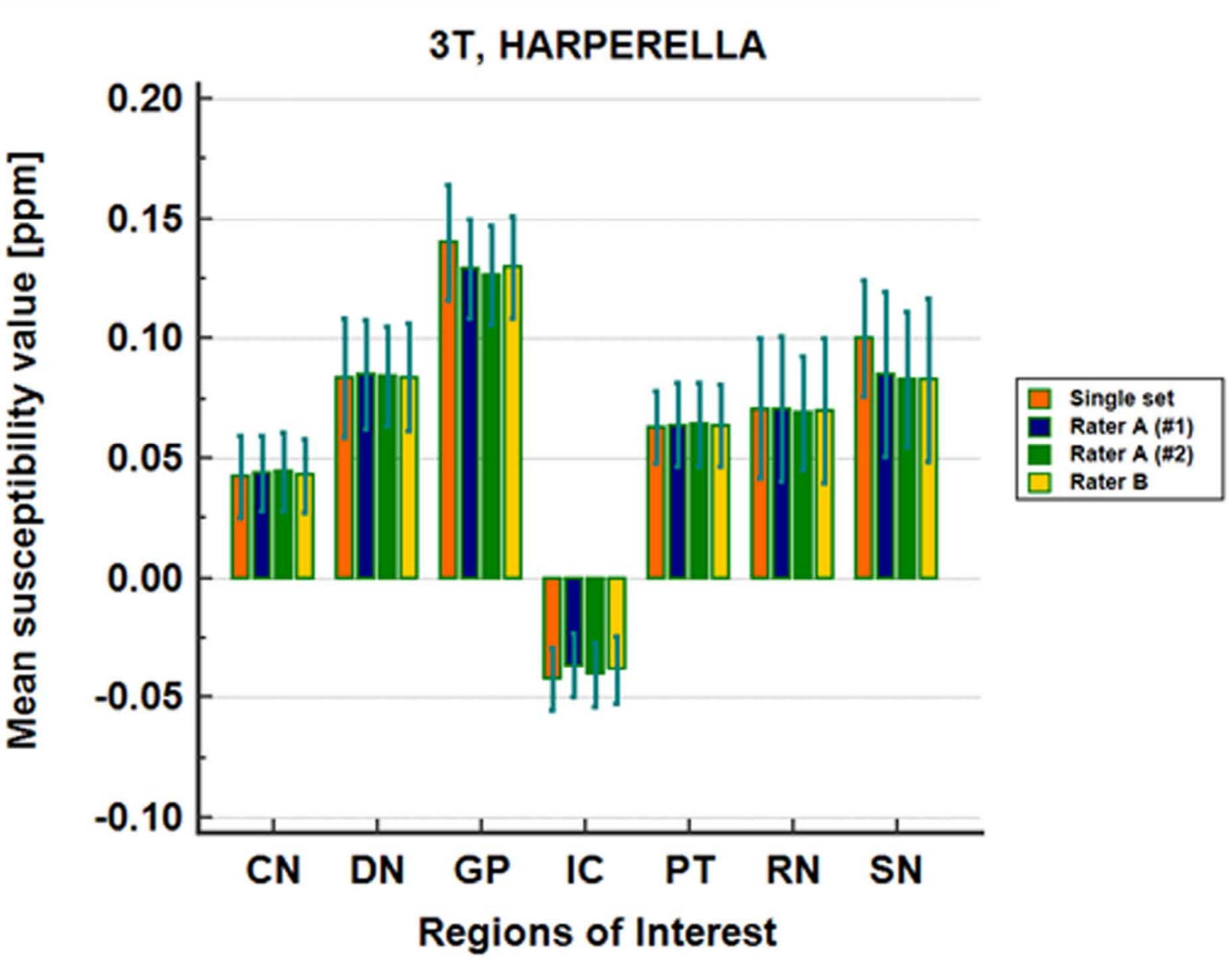

Supplemental Digital Content 2 (a)

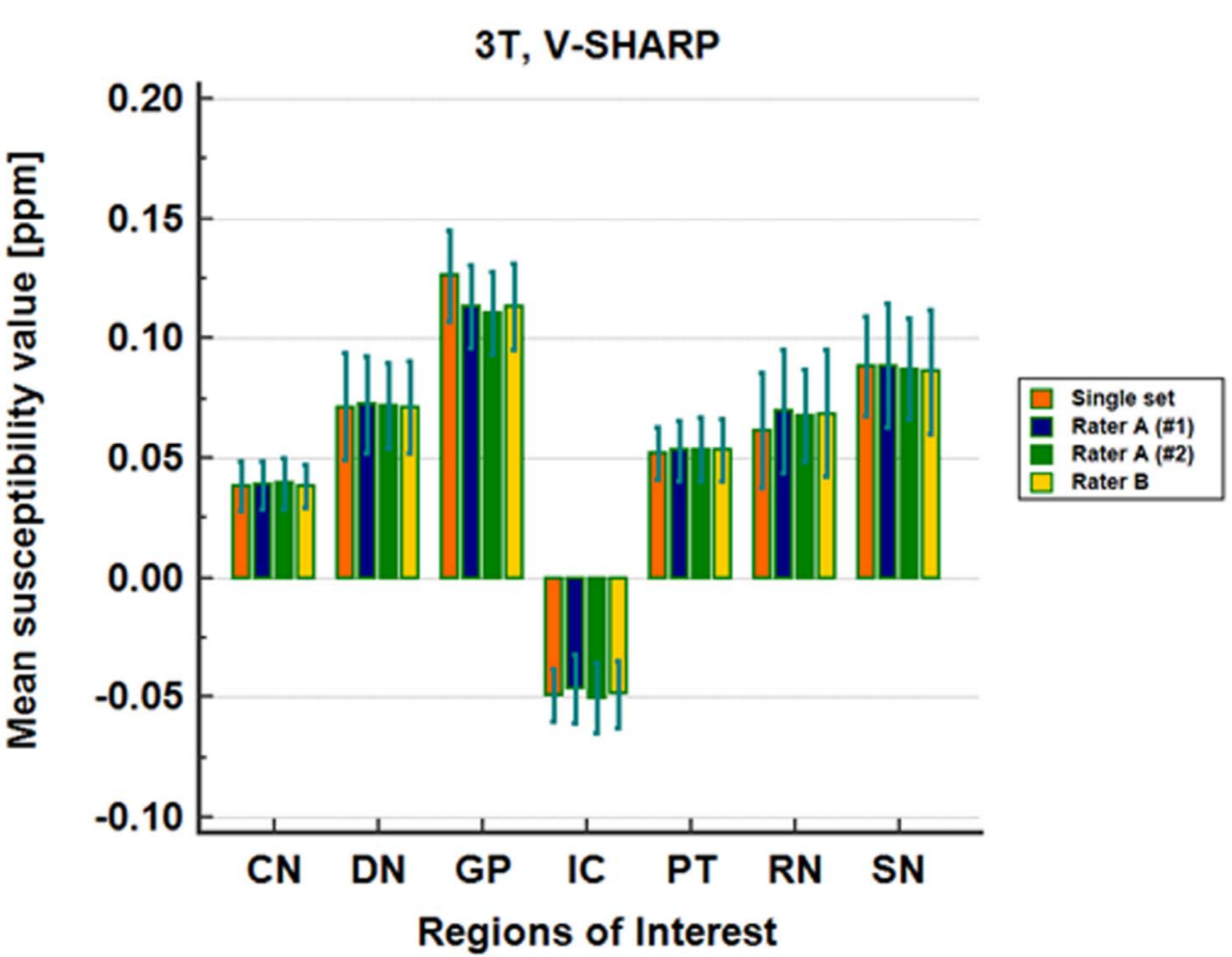

Supplemental Digital Content 2 (b)

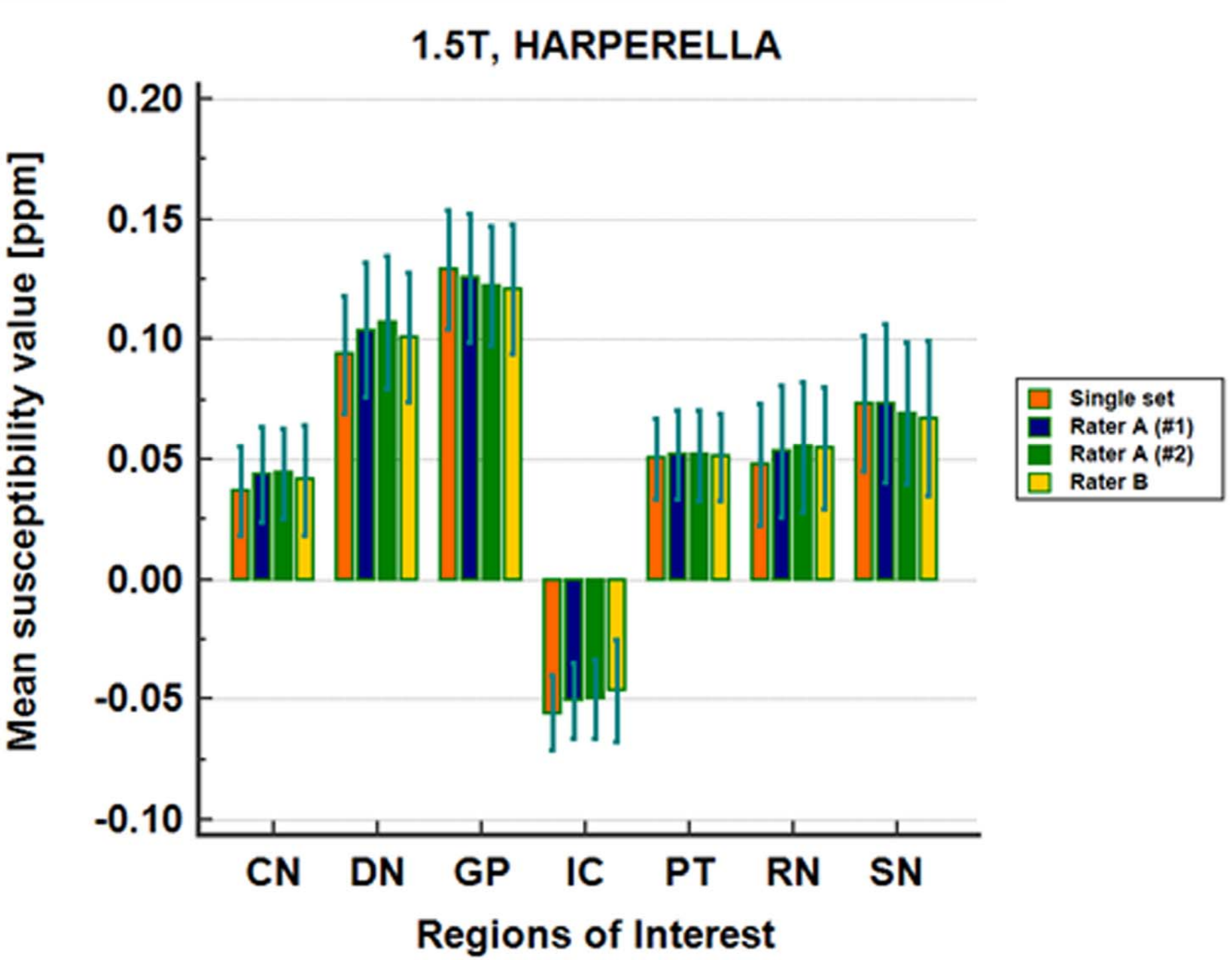

Supplemental Digital Content 2 (c)

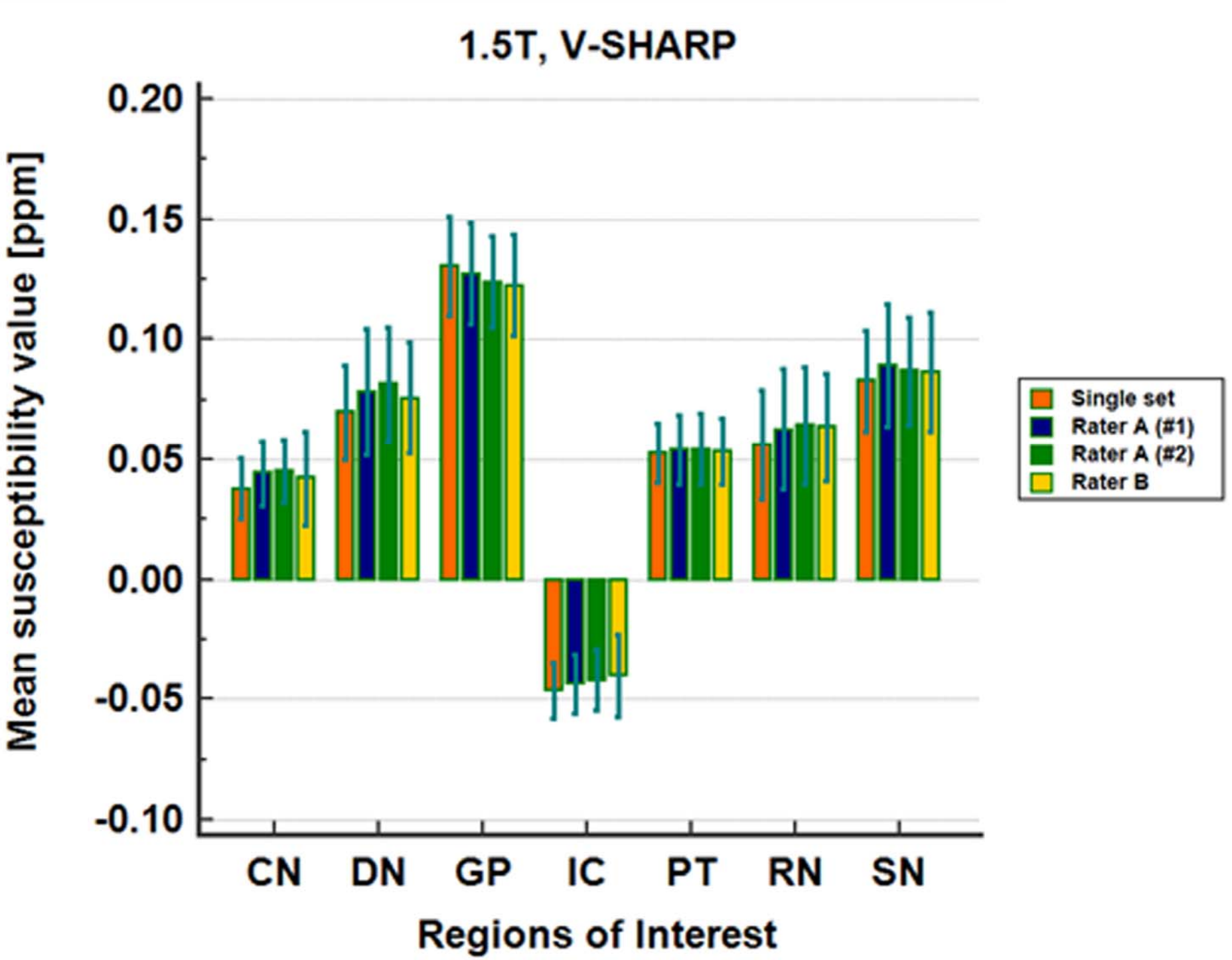

Supplemental Digital Content 2 (d)